

A STUDY OF FREQUENCY DEPENDENT ANALYSES ON
STRATTON OIL FIELD, SOUTH TEXAS

A Thesis Presented to
the Faculty of the Department of Earth and Atmospheric Sciences
University of Houston

In Partial Fulfillment
of the Requirements for the Degree
Master of Science

By

Hazem Ahmed

May 2012

A STUDY OF FREQUENCY DEPENDENT ANALYSES ON
STRATTON OIL FIELD, SOUTH TEXAS

Hazem Ahmed

APPROVED:

Dr. John P. Castagna

Dr. Gennady Goloshubin

Dr. Evgeni Chesnokov

Dr. Robert Schneider

Dean of College of Natural Sciences and Mathematics

Acknowledgments

In any journey one takes in his life, there are companions, friends, and advisers who are always there to help us. There are lots of people who affect our lives, and push us to do better and become better persons.

I would like to express my greatest appreciation to my family, my fiancée, friends, and my professors at the University of Houston who spent their time and efforts trying to help and encourage me.

I would like to extend my gratitude to my committee members, especially Dr. Gennady Goloshubin for all his guidance and support. Also, I'd like to thank Dr. John Castagna for his great advice and support throughout my degree.

I would like to thank CGGVeritas for giving me a free Hampson-Russel workshop. I would also like to thank Dr. Osman Hassan who introduced me to CGGVeritas in the first place. Dr. Osman helped me and guided me a lot, personally and professionally.

I would also like to extend my greatest gratitude and appreciation to Mr. Alejandro Juranovic for helping me throughout my thesis and teaching me about data processing.

At the end, I'd like to thank ExxonMobil that offered me such a great opportunity to pursue a MS degree in Geophysics through the MENA scholarship program.

A STUDY OF FREQUENCY DEPENDENT ANALYSES ON
STRATTON OIL FIELD, SOUTH TEXAS.

A Thesis Presented to
the Faculty of the Department of Earth and Atmospheric Sciences
University of Houston

In Partial Fulfillment
of the Requirements for the Degree
Master of Science

By
Hazem Ahmed
May 2012

ABSTRACT

Frequency dependent analysis has been utilized recently by the industry. It allows the seismic interpreter to see features that could not be clearly seen when dealing with the whole frequency band. This could be related to bed thickness, lithology, or physical properties of the reservoir.

Stratton Oil Field was discovered in 1937, and it is well known to be a highly productive area. At the level of Oligocene Frio Formation, the Stratton field is defined by multiple NW-SW trending structures, like most of the reservoirs along the Gulf of Mexico. The Frio formation is divided into upper, middle, and lower segments. Our study zone lies in the middle and lower segments.

Conventional analysis processes were applied, such as; AVO, inversion, and LMR transform. The investigated zone showed different behavior at each stage of the investigation. Thus, we suggested utilizing a frequency dependent technique to investigate the dataset.

Frequency dependent amplitude analysis was utilized, where anomalous behaviors were indicated at the reservoir zone. Further frequency dependent analyses showed the same anomalous behavior at the reservoir zone. The low frequencies could map the reservoir zone much more obviously, where the anomalies on every stage of the analysis had the same behavior that corresponds to the same zone.

Frequency dependent analysis can help the seismic interpreter to better understand the reservoir characteristics, and can help to map the reservoir anomalies in a better way.

TABLE OF CONTENTS

Introduction	1
Geologic Background	2
1.1 Regional Structural and Stratigraphic Setting of South Texas	3
1.2 Geologic Background of the Stratton-Agua Dulce Field	4
Dataset	6
Data Processing and Preparation	10
3.1 Seismic Data Processing	10
3.2 Well log Preparation and Processing	13
3.3 Seismic-Well Tie	15
Amplitude and Velocity Analysis	17
4.1 AVO and Inversion Techniques	17
4.1.1 AVO Analysis	17
4.1.2 Seismic Inversion	21
4.2 AVO Analysis and Inversion Applications	25
4.2.1 AVO Analysis	25
4.2.2 Post-stack Seismic Inversion	29
4.2.3 Pre-stack Seismic Inversion	32
Frequency Dependent Amplitude and Velocity Analysis	34
5.1 Theory of Frequency Dependence	34
5.2 Upscaling and Filtering	36
5.2.1 Upscaling	36
5.2.2 Data Filtering	39

5.3 Frequency Dependent AVO Analysis	40
5.4 Frequency Dependent Pre-stack Inversion	42
Results	45
6.1 Frequency Dependent Amplitude Analysis	45
6.2 Frequency Dependent Inversion Results	48
Conclusion	55
References	57

LIST OF FIGURES

FIGURE 1-1: Location of the study area. The Stratton oil field extends from northern Kleberg county to southern Nueces county.	3
FIGURE 1-2: Geologic and stratigraphic column of the study area	5
FIGURE 2-1: Acquisition geometry of the 3D seismic survey. The diagram shows the spread of the shot points, receiver stations, binning, and fold.	6
FIGURE 2-2: 3D cube shows the locations of the wells and the deviation paths	7
FIGURE 2-3: Well locations.	7
FIGURE 3-1: Raw shots with applied geometry at FFID 25.	10
FIGURE 3-2: Brute stack image before velocity picking	10
FIGURE 3-3: CDP gathers with TAR, ABA, SCAC, NMO, and time migration	11
FIGURE 3-4: Final post stack image after second velocity picking and second residual, no AGC applied	12
FIGURE 3-5: Well 20. Reservoir zone is shown at 6720 ft (2048 m).	13
FIGURE 3-6: Wavelet extracted from the seismic section. On the left, wavelet time response. On the right, frequency content is shown.	15
FIGURE 3-7: Seismic-Well tie. Correlation coefficient 0.787 between the seismic and the sonic log.	16
FIGURE 4-1: AVO classes (Castagna 1998).	19
FIGURE 4-2: AVO crossplot for various V_p/V_s ratios (Castagna and Swan 1998)	20
FIGURE 4-3: Forward and Inverse modeling (Russel 1991).	21
FIGURE 4-4: Inversion techniques (Pendrel 2001).	23

FIGURE 4-5: Angle gathers, shows that the maximum angle at the zone of interest of 33°.	27
FIGURE 4-6: Intercept section generated from the AVO volume.	27
FIGURE 4-7: Gradient section generated from the AVO volume.	28
FIGURE 4-8: Crossplot intercept vs. gradient.	28
FIGURE 4-9: CDP stacked section, input to the inversion process.	30
FIGURE 4-10: Post-stack initial inversion model.	30
FIGURE 4-11: Inversion error analysis. Correlation between initial model and Final model is 0.99.	31
FIGURE 5-1: On the right, upscaling performed using Backus method. Low frequencies have lower velocities at the reservoir zone. To the right, a diagram with the colors of different logs represented on the left.	38
FIGURE 5-2: Intercept section for the 20Hz-filtered section	41
FIGURE 5-3: Intercept section for the 40Hz-filtered section	41
FIGURE 5-4: Gradient section for the 20Hz-filtered section	41
FIGURE 5-5: Gradient section for the 40Hz-filtered section	41
FIGURE 5-6: Pre-stack inversion model, 10Hz	43
FIGURE 5-7: Pre-stack error analysis. Correlation coefficient between the initial and final model is 0.94.	44
FIGURE 6-1: Intercept and gradient crossplot for the unfiltered section (whole frequency band). No amplitude anomalies noticed at the reservoir zone.	46
FIGURE 6-2: Intercept and gradient crossplot for the 20Hz-filtered section. Amplitude anomalies noticed at the reservoir zone.	47

FIGURE 6-3: Intercept and gradient crossplot for the 40Hz-filtered section. Amplitude anomalies are noticed further to the left of the drilling location.	47
FIGURE 6-4: Post-Stack seismic inversion for the unfiltered section (whole frequency band). An anomaly is revealed at the reservoir location that was not revealed during the AVO analysis.	49
FIGURE 6-5: Elastic impedance inversion for the unfiltered section (whole frequency band). Same anomaly is revealed as on the acoustic impedance volume.	49
FIGURE 6-6: Acoustic wave impedance inversion, 10Hz	50
FIGURE 6-7: Acoustic wave impedance inversion, 20Hz	51
FIGURE 6-8: Acoustic wave impedance inversion, 30Hz	52
FIGURE 6-9: Acoustic wave impedance inversion, 40Hz	53
FIGURE 6-10: Acoustic wave impedance inversion, 50Hz	53
FIGURE 6-11: 10Hz pre-stack inversion volumes. On the left, acoustic wave Impedance volume. In the middle, shear wave impedance volume. On the right, density volume.	54

LIST OF TABLES

Table 2-1: Different types of logs that were included in the dataset with their acronym and unit of measure.	8
Table 2-2: Well location with respect to inline and crossline numbers, and depth of the reservoir zone.	9
Table 5-1: Filtering parameters for every center frequency.	39

LIST OF EQUATIONS

Equation 4-1: Reflection coefficient at a given incident angle.	18
Equation 4-2: Forward model equation in time domain.	22
Equation 4-3: Forward model equation in frequency domain.	22
Equation 4-4: Inverse model equation in frequency domain.	22

Introduction

Frequency dependent analysis has been utilized in the industry for almost a decade now. The need for such analysis was raised up from the need to better map the reservoir zones. Since every frequency responds to certain features in terms of reservoir properties and resolution, therefore the need for better mapping all frequency components becomes more essential to better reservoir mapping.

Stratton oil field was discovered in 1937. At the level of Oligocene Frio Formation, Stratton field is defined by multiple northeast-southwest trending structural closures that are related to deformation of the downthrown block of the down-to-the-coast Vicksburg fault zone. Stratton field extends from northern Kleberg County into Nueces County.

The Stratton field has a huge production rate and many successful wells were drilled. The purpose of this project is to use the frequency dependent analysis to identify the reservoir signature in the successfully drilled wells. Upon identifying the signature, and as the geology of the area in particular structural properties, at the picked horizon (F39 ~6800 ft subsea) does not change much laterally (as opposed to deeper horizons where changes are quite more rapid), we can use this signature to identify the location of the next well to be drilled.

We used conventional velocity and amplitude analysis, and we tried to relate the hydrocarbon saturation to the amplitude or velocity variation. The reservoir zones were not clearly revealed using the conventional analysis, thus we suggested to start with the frequency dependent analysis so we can get a clearer reservoir signature and make it more effective to find the next drilling zone.

Chapter 1: Geologic Background

1.1 Regional Structural and Stratigraphic Setting of South Texas:

The Oligocene Frio Formation is one of the major progradational offlapping stratigraphic units in the northwest Gulf Coast Basin. The Frio Formation is a sediment-supply-dominated depositional sequence, formed at high deposition rates and high subsidence rates (Galloway 1982; Galloway 1991).

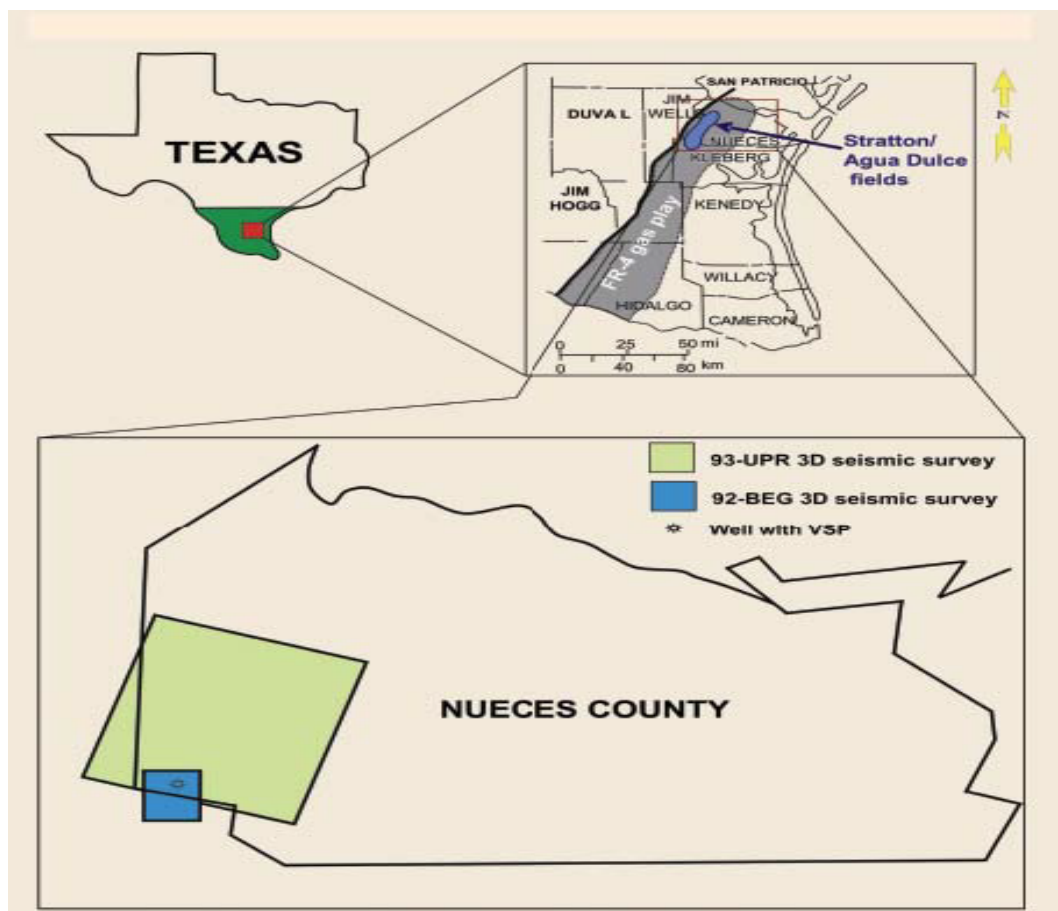


Figure 1-1: Location of the study area.

1.2 Geological Background of the Stratton-Agua Dulce Field:

The Oligocene Frio Formation is divided into three operational units; the lower, middle, and upper. The lower Frio consists of 10 to 40 ft (3-12 m) thick continuous sandstones. The lower Frio is 500 ft (152 m) thick along the crest of the structure that defines Stratton field. The thickness varies as we move northwest into the Vicksburg fault zone and southeast toward the Gulf of Mexico.

The middle Frio Formation is defined as the interstratified mudstones and lenticular sandstones resting above and in marked contrast to the sandstones of the lower Frio Formation. The middle Frio Formation is 2,500 ft (762 m) thick, but the thickness varies because the contact with the lower Frio is stratigraphically transitional over a few hundred feet vertically. Laterally stacked sandstones lead to “leaky” reservoir compartments. Vertically stacked sandstones lead to more “isolated” reservoir compartments.

Our area of interest falls between the middle and lower Frio formation, where we target reservoir F39 (~ 6800 ft; 2072 m subsea). The middle Frio formation is composed of fluvial deposits in the form of point bar and crevasse splay sandstones isolated within floodplain mudstones and siltstones. This heterogeneity makes it possible that even small vertical fault offsets along these faults may form lateral flow barriers. Another way in which these synthetic and antithetic faults may compartmentalize the middle Frio

reservoirs is by providing seals, which follow the fault as gouge or cemented breccia, which formed along fault movement.

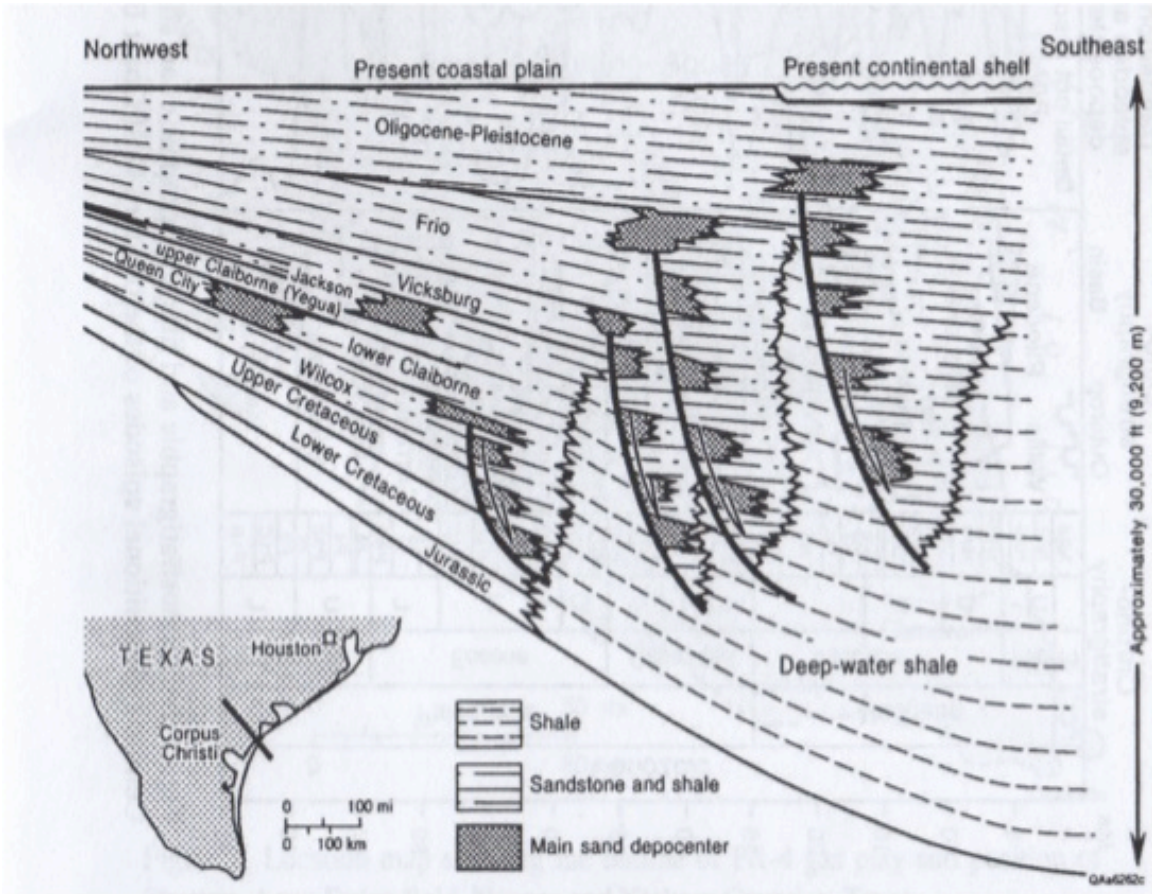


Figure 1-2: Geologic and stratigraphic column of the study area.

Chapter 2: Dataset

We received the Stratton field data set from the BEG (Bureau of Economical Geology) at University of Texas, Austin. The 3-D source/receiver geometry consisted of east-west receiver lines spaced 1320 ft apart, and north-south source lines spaced 880 ft apart. Linear, 12-element receiver arrays were constructed so each array spanned 110 ft. The distance between the centers of adjacent arrays was 110 ft. Vibrator points (VP's) were spaced at intervals of 220 ft. Six sweeps from four inline vibrators were summed at each VP. A linear, 8-120Hz sweep rate was used, and the sweep length was 14s.

The receiver spacing of 110 ft and the source spacing of 220 ft created an acquisition bin of 55 ft by 110 ft. The data volume comprises 100 inlines (oriented east-west) and 200 crosslines (oriented north-south). The crossline length is 3s, and the sample rate is 2ms. Trace spacing is 55 ft both from east to west and from north to south.

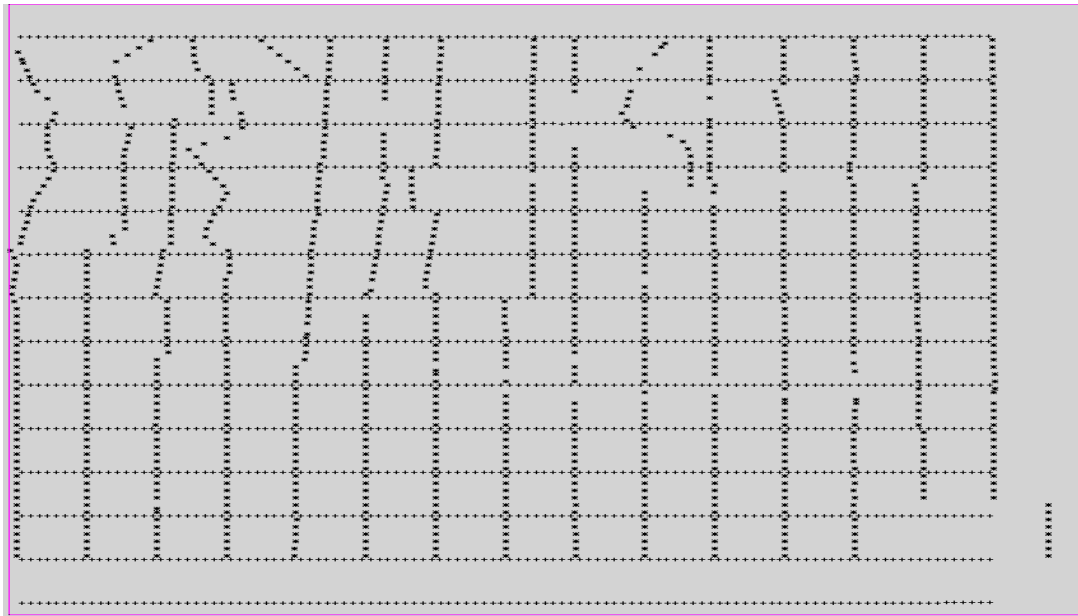


Figure 2-1: Acquisition geometry of the 3D seismic survey.

Studying the dataset we found the reservoir zone of particular interest to be zone F-39. Reservoir F-39 is extended through all the wells except well 1. Using the SP and GR logs to define the best reservoir zone to work on, all wells were plotted on Hampson-Russell and compared to each other along with their referred location on the base map. It appeared that wells 9 and 20 had the best reservoir zone from the thickness point of view. Well 9 is mapped to fall on inline 79 and crossline 89 on the seismic section, and well 20 is mapped to fall on inline 75 and crossline 109.

ACRONYM	UNITS	Type of Well Log
SP	Ohm-m	Self Potential
GR	API	Gamma Ray
SN	mV	Shot Normal Resistivity
ASN	Ohm-m	Amplified Short Normal
LAT	Ohm-m	Lateral
MINV	Ohm-m	Microinverse log
MNOR	Ohm-m	Micronormal log
RT	Ohm-m	True Resistivity
ILM	Ohm-m	Medium Induction log
ILD	Ohm-m	Deep Induction log
SFLU	Ohm-m	Spherically Focused log
NPSS	Porosity units	Neutron Porosity Sandstone
RHOB	g/cc	Bulk Density
GRD	Ohm-m	Guard
SGRD	Ohm-m	Shot Guard
CALIPER	Inches	Caliper
DRHO	g/cc	Density Correction
LN	Ohm-m	Long Normal

Table 2-1: Different types of logs that were included in the dataset with their acronym and unit of measure.

Well no.	Inline (EW lines)	Crossline (NS lines)	X	Y	F39 SL datum (ft)	F39 Two-way time (ms)
1	94	60	2190500	710610	N/A	N/A
2	76	127	2186815	709620	6585	1639
3	24	124	2186980	706760	6632	1649
4	24	106	2187970	706760	6635	1649
5	40	110	2187750	707640	6651	1652
6	19	55	2190775	706485	6730	1668
7	88	154	2185330	710280	6584	1639
8	67	154	2185330	709125	6656	1653
9	79	89	2188905	709785	6611	1644
10	37	158	2185110	707475	6699	1662
11	53	89	2188905	708355	6636	1649
12	54	39	2191655	708410	6756	1673
13	32	76	2189620	707200	6671	1656
14	16	178	2184010	706320	6697	1661
15	3	121	2187145	705605	6663	1655
16	83	64	2190280	710005	6688	1660
17	29	36	2191820	707035	6789	1680
18	51	54	2190830	708245	6719	1666
19	3	154	2185330	705605	6721	1666
20	75	109	2187805	709565	6600	1642
21	3	40	2191600	705605	6757	1673

Table 2-2: Wells location with respect to inline and crossline numbers, and the depth of the reservoir zone.

Chapter 3: Data Processing and Preparation

3.1 Seismic Data Processing

The processing of the seismic data was started by creating the geometry. Geometry was extracted from the swath files. Binning was applied to fit the best fold, CMPs were created, and geometry was QCed to ensure correct geometry application before proceeding with further processing.

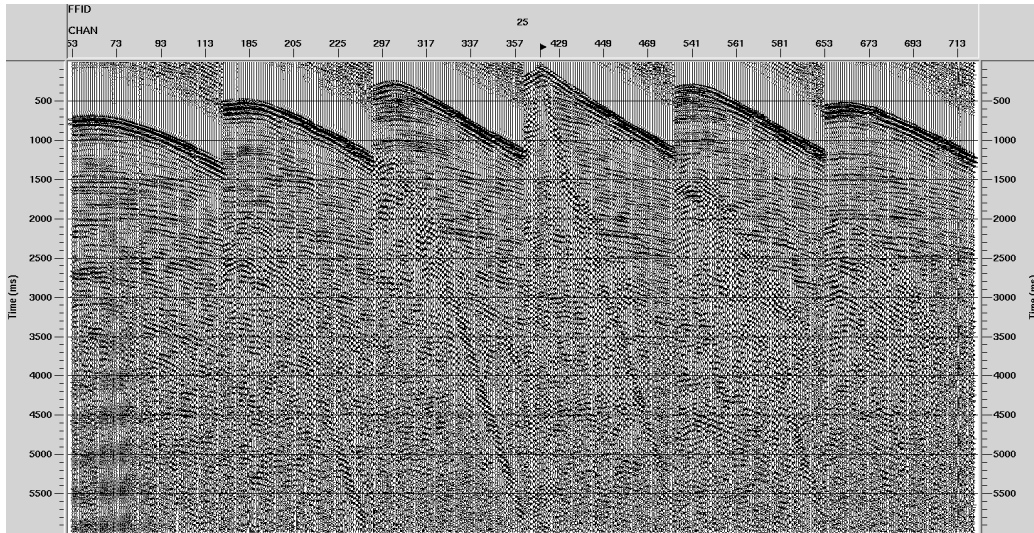


Figure 3-1: Raw shots with applied geometry.

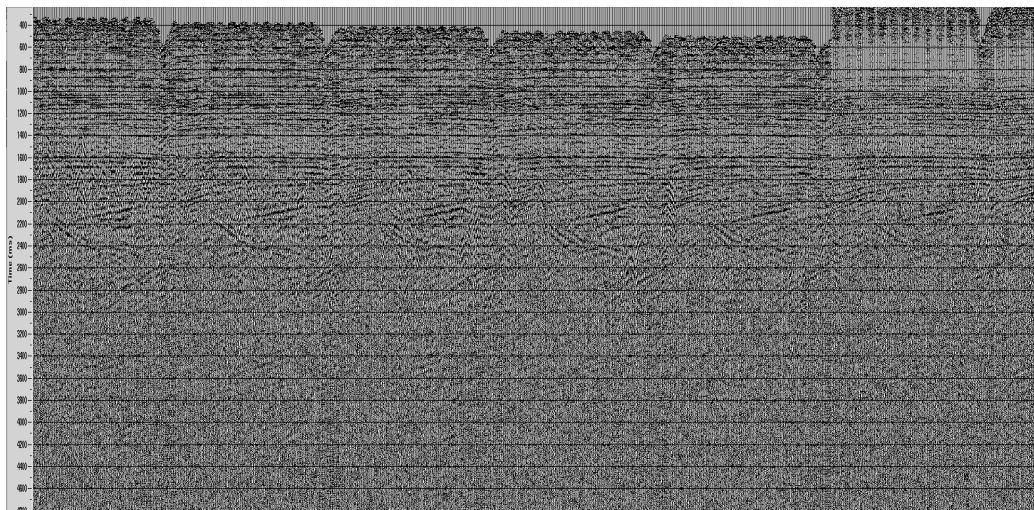


Figure 3-2: Brute stack image before velocity picking.

CDP gathers were created after further trace editing and muting. Pre-processing was performed to ensure a preserved amplitude and frequency processing; True Amplitude Recovery (TAR), Air Blast Attenuation (ABA), and Surface Consistent Amplitude Compensation (SCAC). Brute velocity analysis was performed to produce a brute stack image.

First residual statics and first velocity picking helped to improve the image. Second residual statics and second velocity picking produced remarkable results. Pre-stack time migration was performed to produce CDP gathers that ensure a correct amplitude analysis. Barely filters were used to reduce the Signal-to-Noise Ration (SNR).

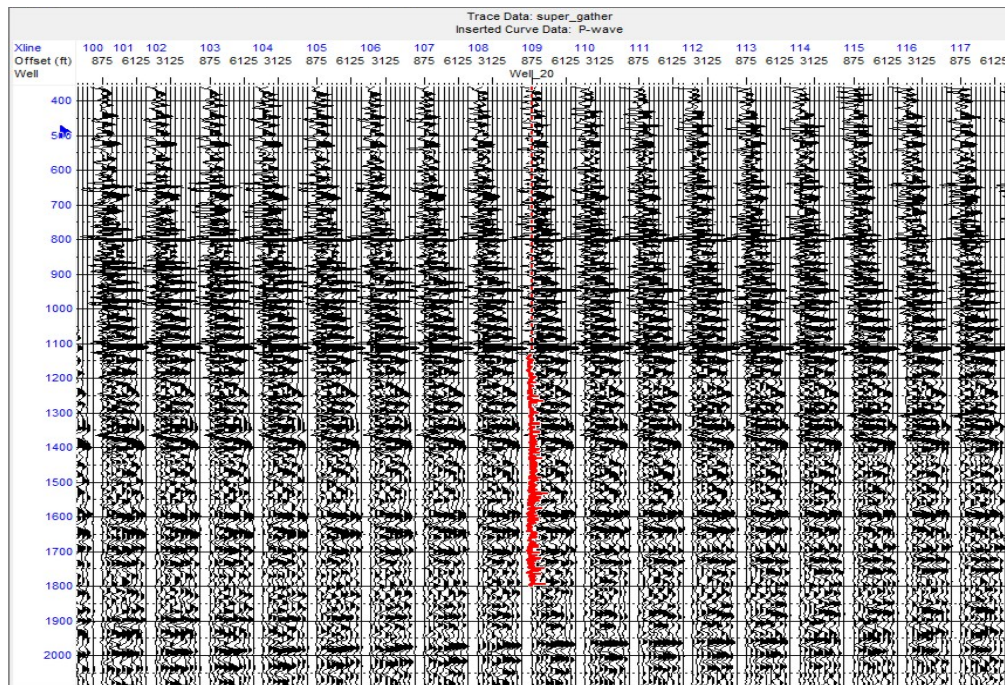


Figure 3-3: CDP gathers with TAR, ABA, SCAC, NMO, and time migration.

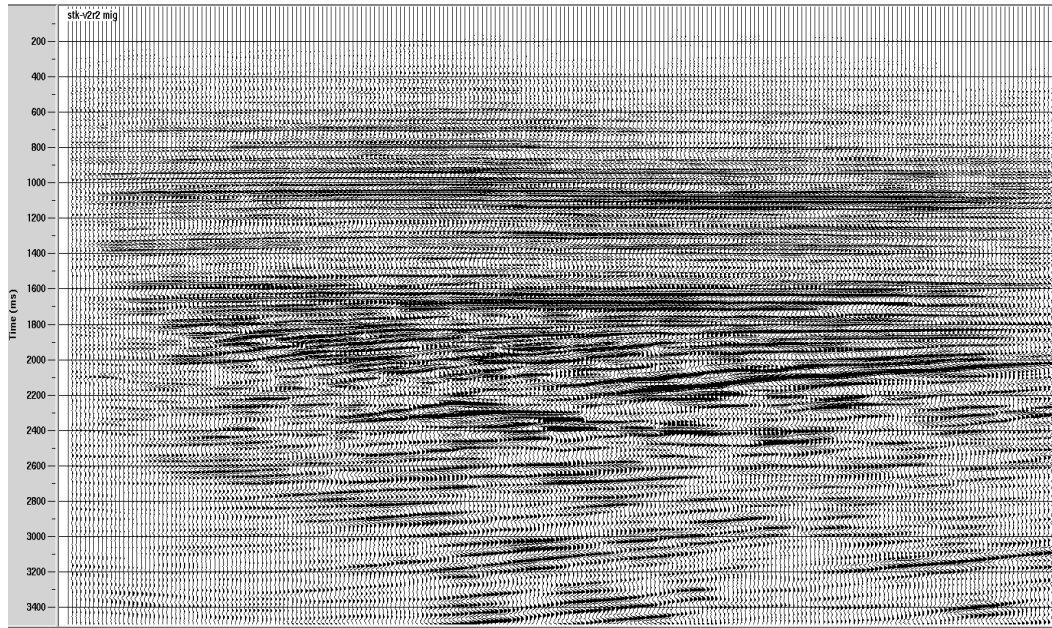


Figure 3-4: Final post stack image after second velocity picking and second residual, no AGC applied.

The output of the seismic processing was used for creating sonic logs, well-seismic tie, and AVO analysis. At this stage we have CDP output gathers, and post-stack migration sections. The data was cut to reduce its size to the range of 70-80 inlines and all the crosslines were included. Cutting the data helped to reduce the processing time for further processes including AVO analysis and inversion processes specially the pre-stack inversion, which is a time consuming process.

3.2 Well Log Preparation and Processing

Well logs were loaded into Hampson-Russell software for analysis and further processing. The wells given were loaded to create a base map of the wells with respect to (X, Y) coordinates.

Using elog module, sonic logs were created using available information (resistivity and density logs). We used the Faust's equation and the reversed Gardner's equation to compute the sonic logs.

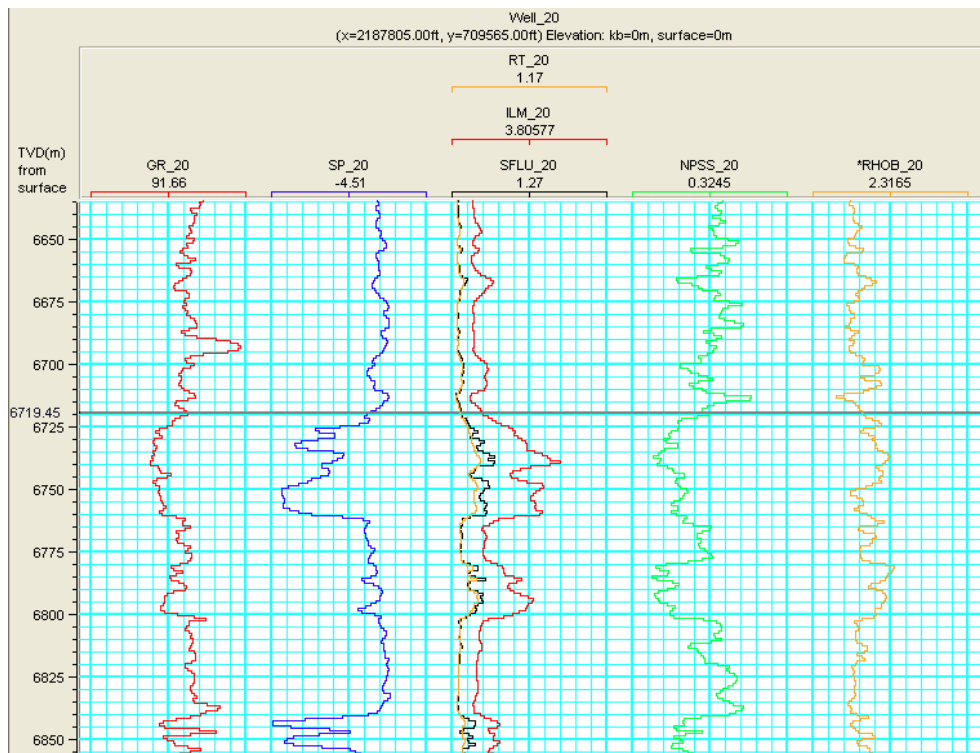


Figure 3-5; Well 20. Reservoir zone is shown at 6720 ft (2048 m).

The parameters used in Faust's equation and Reversed Gardner's equation, were tweaked to match the depth of the target zone with the corresponding seismic event using the time-depth curve. We noticed that the Faust relation gave a higher velocity, while the Gardner average equation produced a lower velocity than expected. An average was taken to smooth the depth-time curves to best tie the well logs to the corresponding events on the seismic data.

Well log correlation and interpretation was performed to define the best reservoir zone to focus on during this project. Reservoir zones were determined through a correlation of SP and GR logs from all wells with the suggested location within the data. We tried to calculate water saturation in all the wells, but due to some missing information like mud filtrate resistivity we were not able to precede. Another way was to calculate relative water saturation in all the wells related to one of the 21 wells. In order to calculate water saturation; we had to calculate formation factor, temperature of the formation (using a temperature gradient $G=1.9$ F/100 ft as the temperature gradient trend ranges from 1.7 F/100 ft to 2.2 F/100 ft as we move from near coast to south-central Texas; Rae and Roemer, 1990). The temperature dependent coefficient, K was calculated with the given information, then the formation factor was calculated using Humble best average for sands equation. Some of the wells were missing the porosity log; as a result water saturation could not be calculated in these wells. Another way was to look at the proposed reservoir horizon, and the available wells; Reservoir F39 did not spread out to well 1 due to stratigraphic conditions (absence of a seal due to faulting).

3.3 Seismic-Well Tie:

After processing the data and generating a sonic log that matches the corresponding reservoir zones from logs to their seismic locations, a seismic-well tie was performed. We extracted several wavelets using different parameters from the seismic section and used them to correlate the seismic and the well logs together using Hampson-Russell software. A correlation coefficient of 0.767 was achieved after stretching and applying minimal time shifts, using a wavelet that is extracted from the time section 1300-1800ms with a 200ms wavelength. That was the highest correlation we could achieve after several trials.

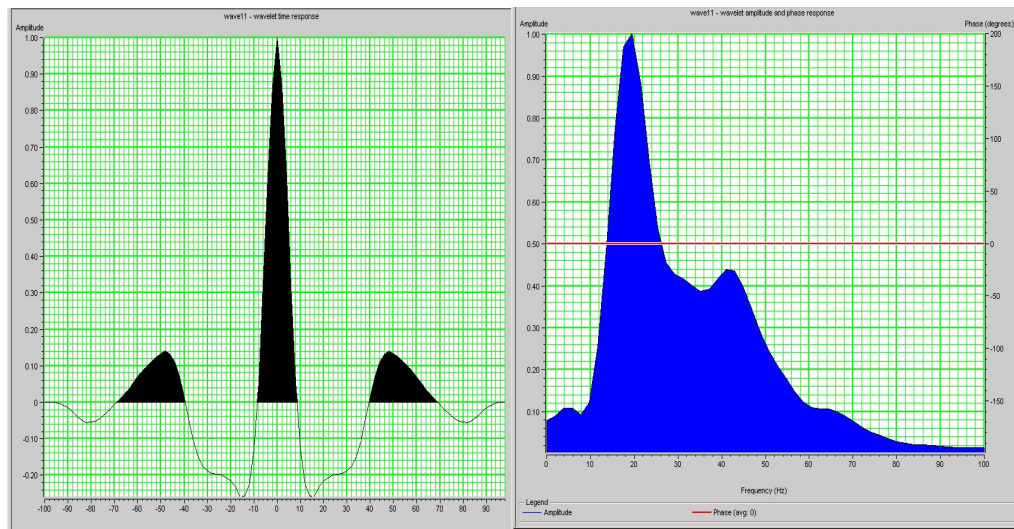


Figure 3-6: Wavelet extracted from the seismic section. On the left, wavelet time response. On the right, frequency content is shown.

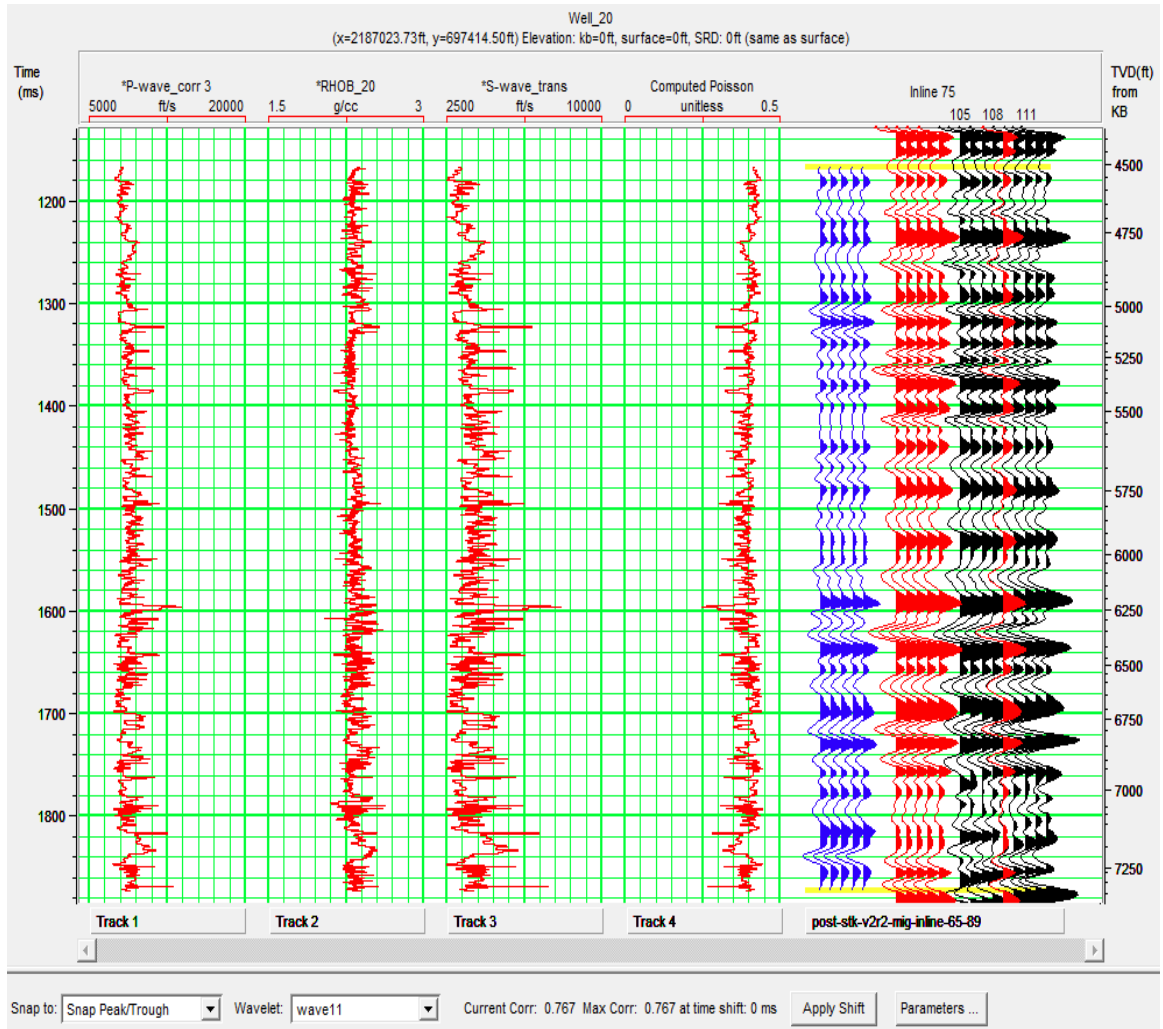


Figure 3-7: Seismic-Well tie. Correlation coefficient 0.787 between the seismic and the sonic log.

Chapter 4: Amplitude and Velocity Analysis

After data preparation and processing to produce CDP gathers and post-stack seismic sections, and well log editing and correlation, we are ready to proceed to the amplitude analysis step. For such analysis we have utilized AVO and inversion techniques.

4.1 AVO and Inversion Techniques:

4.1.1 AVO Analysis:

AVO (amplitude variation versus offset) analysis goes back to the 1980s. Ostrander in 1984 noticed that the variation of P-wave reflection coefficients at an interface vary with angle of incidence and depends on type of saturation.

Prior to the 1970s, a seismic interpreter would have looked only at structure and propose to drill the first bright spot he sees. Many wells were drilled this way of which some were unsuccessful. The foundation of AVO analysis goes back to the Zoeppritz equations.

The Shuey's approximation is the one widely used to express AVO anomalies. In the Shuey's equation; the traces of a seismic gather reflect away from the boundary with an incident angle θ .

The first order approximation is given by equation 4.1:

$$R(\theta) = R_o + B \sin^2(\theta) \dots \text{Eq. 4.1}$$

where $R(\theta)$ is the reflection coefficient at an incident angle θ .

R_o is the zero offset reflection coefficient.

B is the gradient (slope), which produces the AVO response.

AVO uses the difference between V_p and V_s to try to detect changes primarily in the pore fluid, as well as lithologic settings. Different AVO anomalies develop due to different geologic settings (upper and lower impedance relative to the reflection boundary). There are four classes for AVO anomalies that indicate the presence of hydrocarbons at the reservoir. These classes are based on the zero-offset reflection coefficient and the gradient.

Class 1 is referred to as “Dim Spot” where there is a large positive reflection at the top of the reservoir and the amplitudes decay as the angle of incidence increases (Shale to sand; softening).

Class 2 is referred to as “Phase or Polarity Reversals” where there is a small positive reflection coefficient on top and then converts to negative amplitude as the angle of incidence increases.

Class 3 is referred to as “Bright Spot” where there is a negative reflection on top of the reservoir and the amplitudes becomes more negative with the increase of the angle of incidence.

Class 4 is similar to class 3 but with much slower decrease in the amplitude with the increase of the angle of incidence

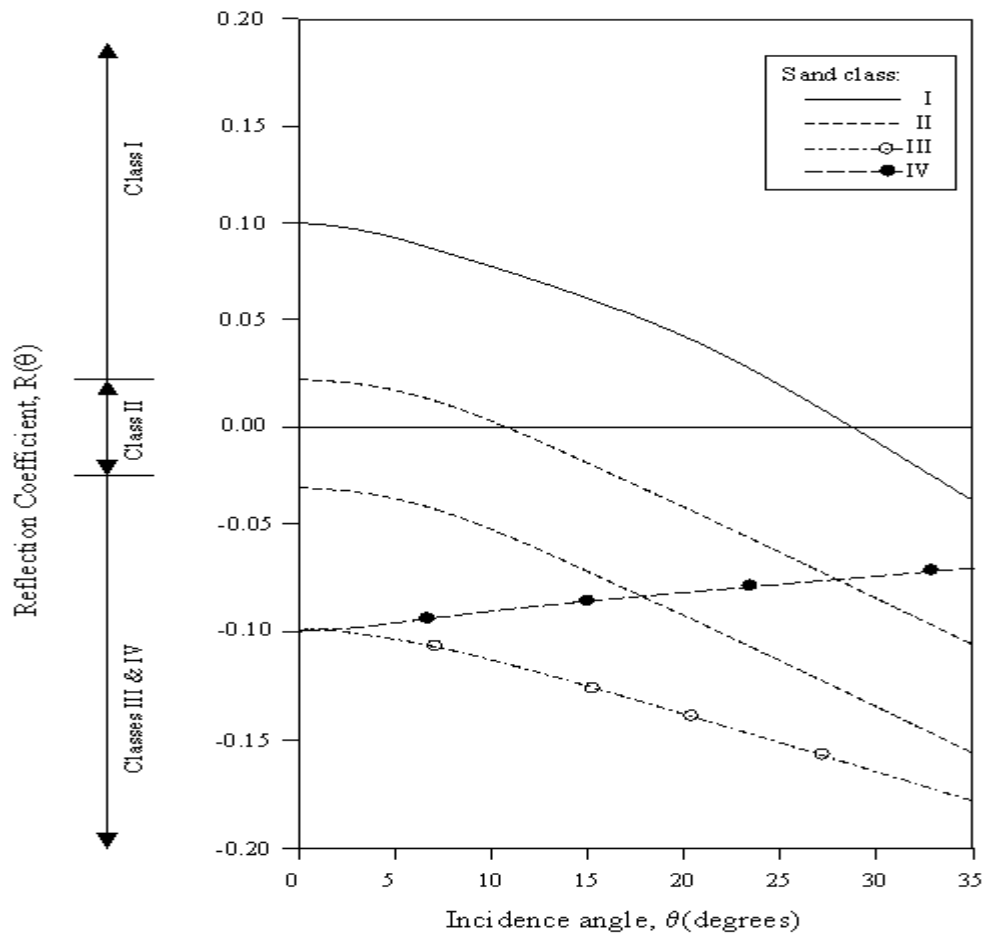


Figure 4-1: AVO classes (Castagna 1998).

The classification and identification of AVO classes anomalies, does not directly imply that we are dealing with hydrocarbons. The AVO classes were originally defined for gas sand, but we might be dealing with a type of amplitude anomaly that classifies as an AVO class, yet it is not related to hydrocarbons.

The AVO cross plotting was developed along the past two and half decades. Castagna (1997) proposed a very simple way to plot the anomalies. He suggested that the top reflections should be plotted in the 4th quadrant, and they all follow a background trend. The V_p/V_s ratio will govern the slope of the background trend. This way was followed in this project for plotting the AVO anomalies.

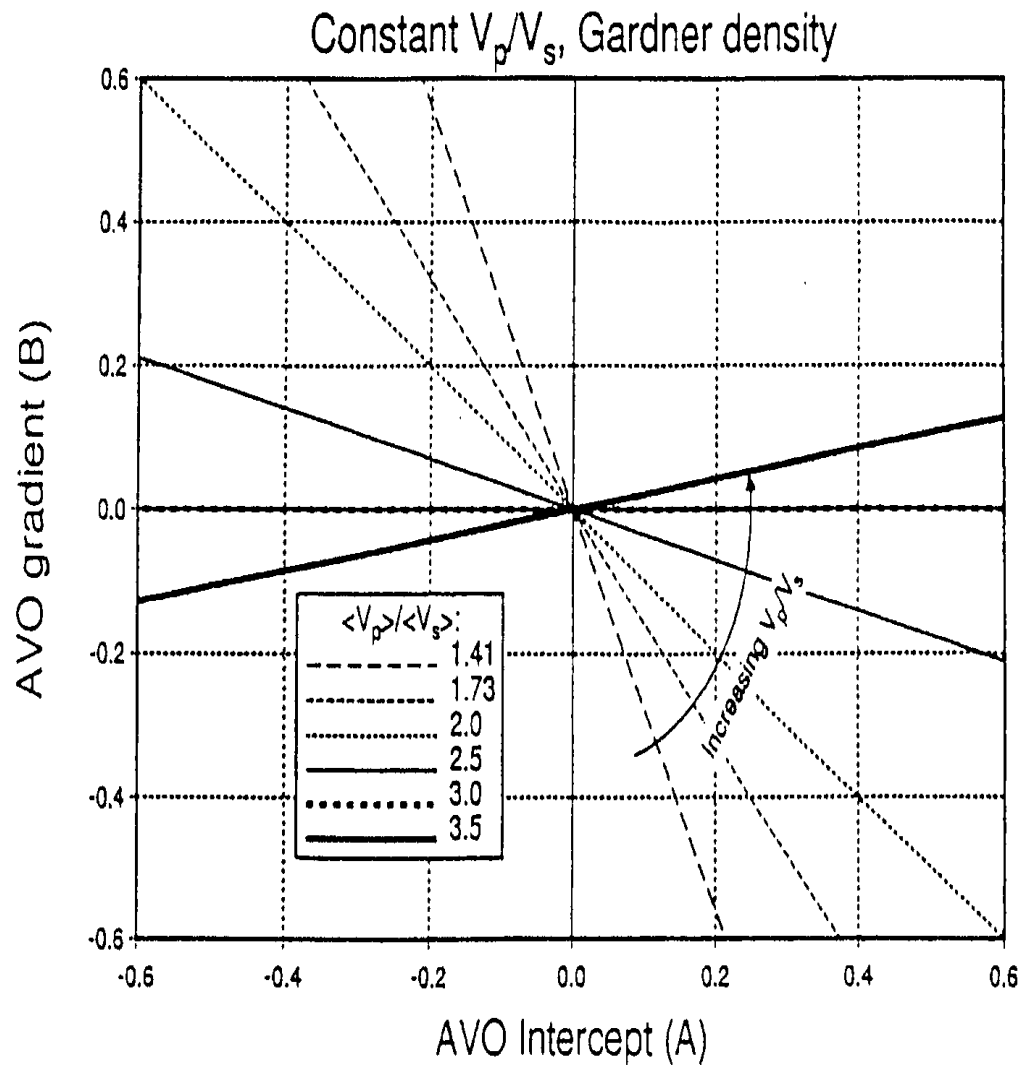


Figure 4-2: AVO crossplot for various V_p/V_s ratios (Castagna and Swan, 1998).

4.1.2 Seismic Inversion:

Inversion is the process utilized by geophysicists to map and develop the physical structures of the subsurface using seismic (surface) measurements. We can also define Inversion as a way to create a model of the earth using the seismic data as input.

In such a way, inversion can be considered the opposite of the forward modeling technique, which involves creating a synthetic seismic section based on an earth model and/or using well logs as priori information that is needed for the inversion process from a mathematical point of view.

The forward model uses a pre-existing earth model, and with the utilization of some model processing algorithms we can create the seismic response from such model. The inverse model is just the opposite, where we start by the seismic response and we try to create the earth model.

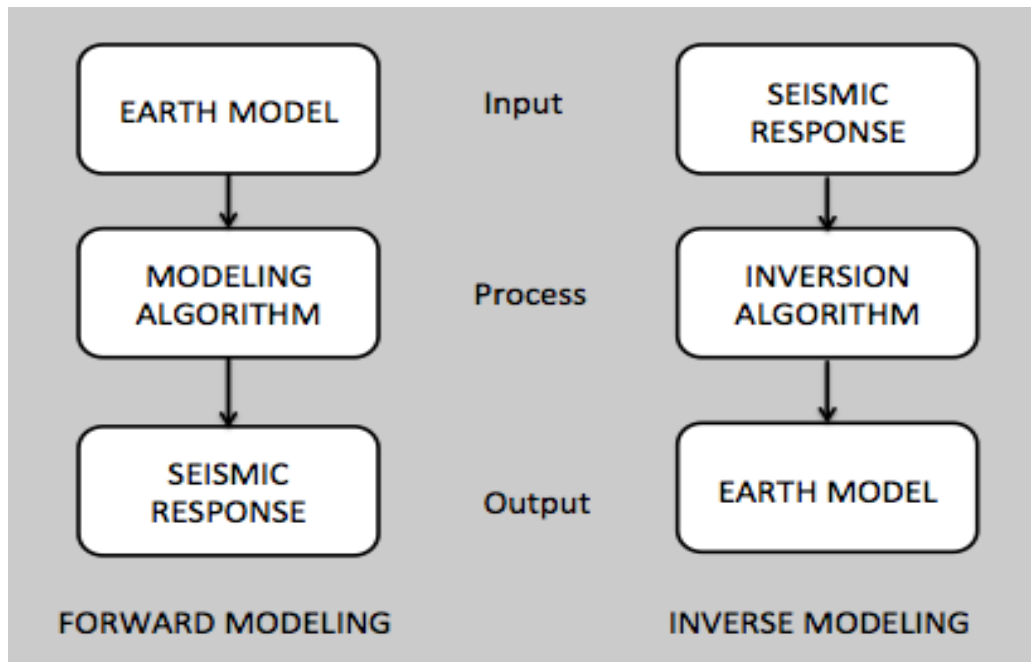


Figure 4-3: Forward and inverse modeling (Russel, 1991).

The seismic trace in both time and frequency domains consists of three components; reflectivity, seismic wavelet, and noise.

The forward model can be expressed using equation 4.2:

$$S(t) = W(t) * R(t) + N(t) \dots \text{Eq. 4.2}$$

where $S(t)$ is the output seismic trace.

$W(t)$ is the wavelet used to create the seismic model.

$R(t)$ is the reflectivity series from the pre-existing model.

$N(t)$ is noise.

In the frequency domain this equation can be expressed as:

$$S(w) = W(w).R(w) + N(w) \dots \text{Eq. 4.3}$$

In such a manner, while forgetting about noise for simplicity, the reflectivity series can be expressed as:

$$R(w) = S(w)/W(w) \dots \text{Eq. 4.4}$$

The last equation expresses the process of inversion, where we try to extract information about the earth model using only surface measurements (seismic model). It is clear that a result of the inversion depends on signal to noise ratio.

Many algorithms exist in the business today for the inversion process; Model-based Inversion, Sparse-Spike Inversion, etc. The basic differences among these methods are algorithm stability, processing time, and ability to produce a better vertical resolution while maintaining the quality of the horizontal resolution.

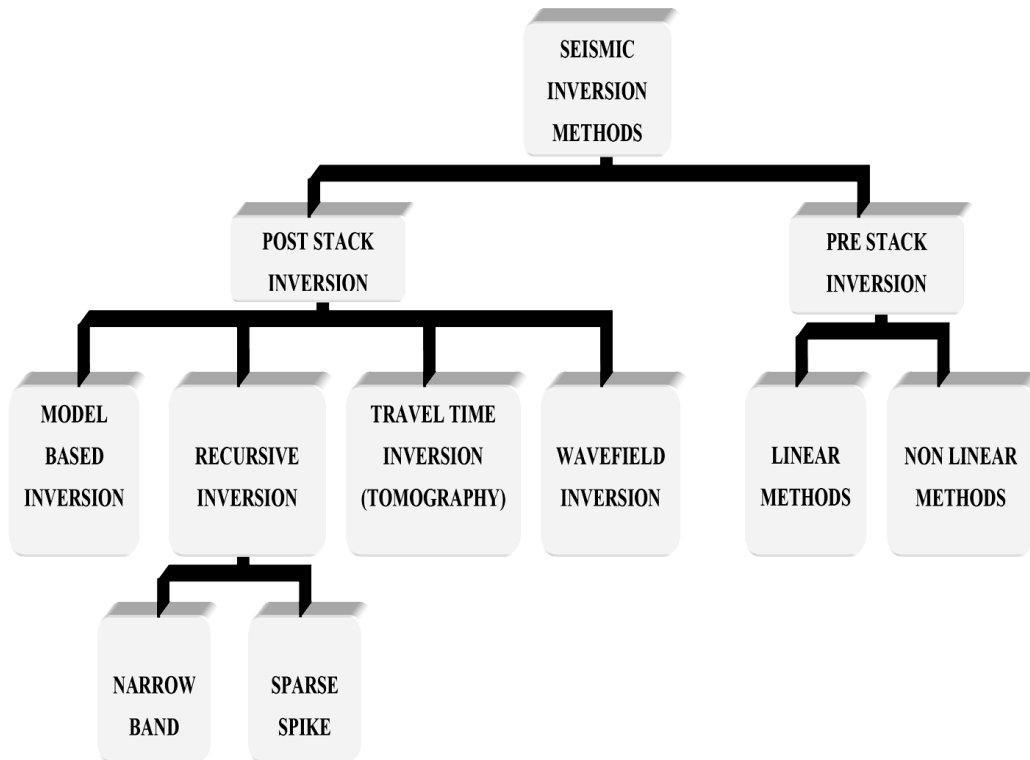


Figure 4-4: Inversion techniques (Pendrel, 2001).

The Model-based Inversion, which we used for our project, is a type of inversion, where a geological model is iteratively updated to find the best fit with the seismic data.

The final output of seismic inversion is impedance; it means that all our aim is to build an impedance model. A good quality impedance model contains more information than seismic data; it contains all the information in the seismic data without the complicating factors caused by wavelets, and adds essential information from the log data.

An impedance volume is a result of the integration of data from several different sources, typically seismic, well log, and/or velocity. An impedance model is the most natural way to integrate data and provide a model that could be understood by geologists, geophysicists, petrophysicists, and engineers. Using integration reduces the effects of wavelet tuning and therefore the resolution of seismic data is improved, enabling the model to have a better vertical resolution, where events can be clearly shown. Random noise is highly attenuated, which makes the interpretation process much easier.

Impedance is a rock property; it is the product of density and velocity, both of which can be directly measured by well logging. Seismic data are interface properties, a close approximation to the convolution of a wavelet with a reflection coefficient series, which reflects relative changes in impedance. In such a manner, the impedance model acts as a link between surface measurements (seismic data), and subsurface measurements (logs).

Impedance is closely related to lithology, porosity, pore fill, and other factors. It is common to find strong empirical relationships between acoustic impedance and one or more of these rock properties. Impedance is a layer property; Seismic amplitudes are attributes of layer boundaries, which makes it easier to perform sequence stratigraphic analysis. Wavelet side lobes are attenuated, eliminating some false stratigraphic-like effects.

The inversion process is utilized to handle angle or offset stacked data to produce elastic impedance model. Elastic impedance captures AVO information and, in conjunction with AI, improves interpretation power and the ability to discriminate lithology and fluids.

4.2 AVO Analysis and Inversion Applications:

4.2.1 AVO Analysis:

After the seismic data were processed using amplitude and frequency preserving techniques, we were ready to use the output CDP gathers to perform the AVO analysis. The CDP gathers were loaded into the Hampson-Russell software to use the AVO module for our analysis.

Our analysis steps on Hampson-Russell AVO module are as following:

1. Start a single well AVO model. For this step we chose one of the two wells we would like to focus on. We chose well 20 and started an AVO modeling for this well.
2. Using the CDP gathers, we create a super gather. The main aim of the super gather is to enhance the SNR by reducing random noise. We created a super gather using every 10 crosslines. We also created a CDP stack to use it later on for post-stack analysis.
3. Using the seismic section, we extract the wavelet that will be used to correlate the seismic and the logs. We extracted a 200ms wavelet from the interval 1300-1800ms. This wavelet could achieve a correlation coefficient of 0.76 between the seismic and the logs.
4. After correlation and adjustment of the logs, we use the sonic log to create angle gathers. Angle gathers will be used later on for the elastic inversion. We found that the maximum angle at the zone of interest is 33°.

5. We start the AVO analysis by creating an AVO attribute volume. The first step is to view the pick analysis. We pick a horizon and view how the amplitudes change across it. This could give us an idea of the AVO anomaly we are about to encounter.
6. We start the gradient and intercept analysis. We set the AVO attribute volume to be viewed as intercept and gradient volumes. This step can help us identifying the anomaly location and will help us while cross plotting the anomalies.
7. After creating the intercept and gradient volume, we need to crossplot the seismic section at the specific horizons where the anomalies exist to identify what class this AVO anomaly is. We crossplot intercept versus gradient and use the Castagna method of cross-plotting. We had class III anomalies (also known as bright spots). Then we define filter zones on the cross plot where we used the red color for gas sands, blue for brine sands, and grey for shale. These zones were then used as DHI indicators on the CDP stacked section to view the location of the class III anomalies we just identified.

Following these steps helped to identify and crossplot the amplitude anomalies we observed on the dataset we had.

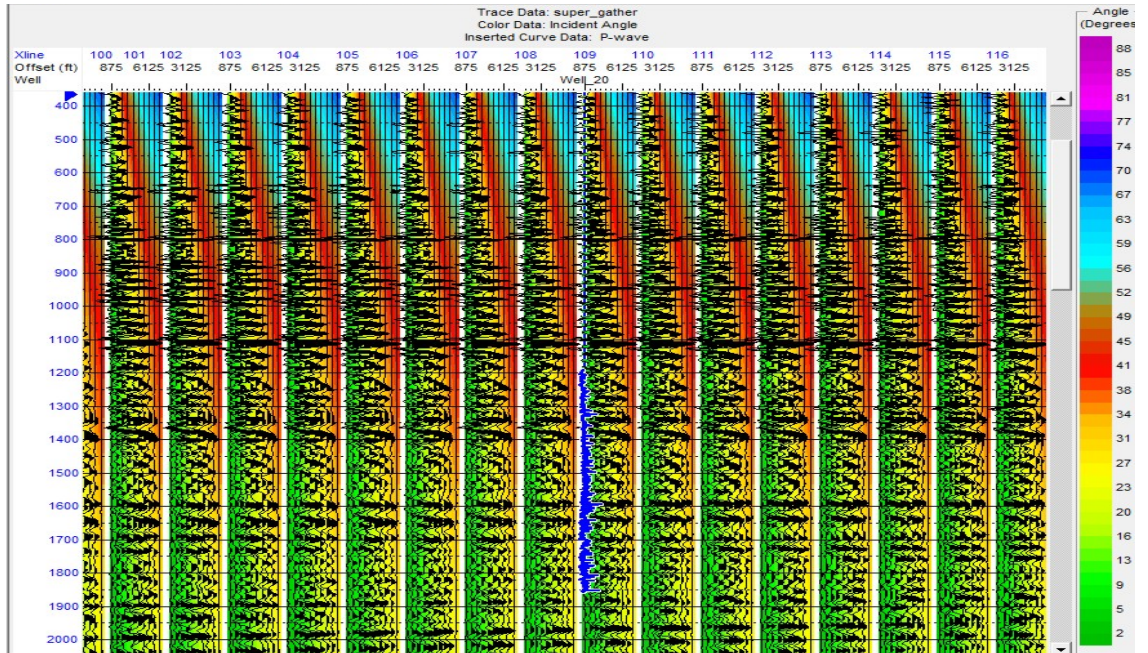


Figure 4-5: Angle gathers, shows that the maximum angle at the zone of interest is 33°.

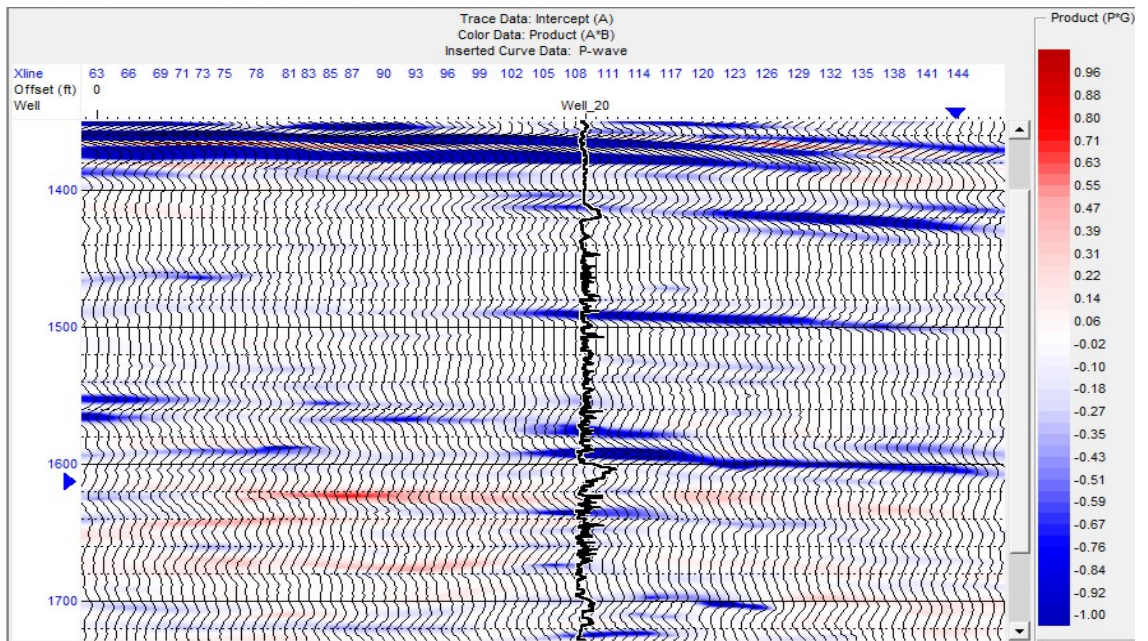


Figure 4-6: Intercept section generated from the AVO volume.

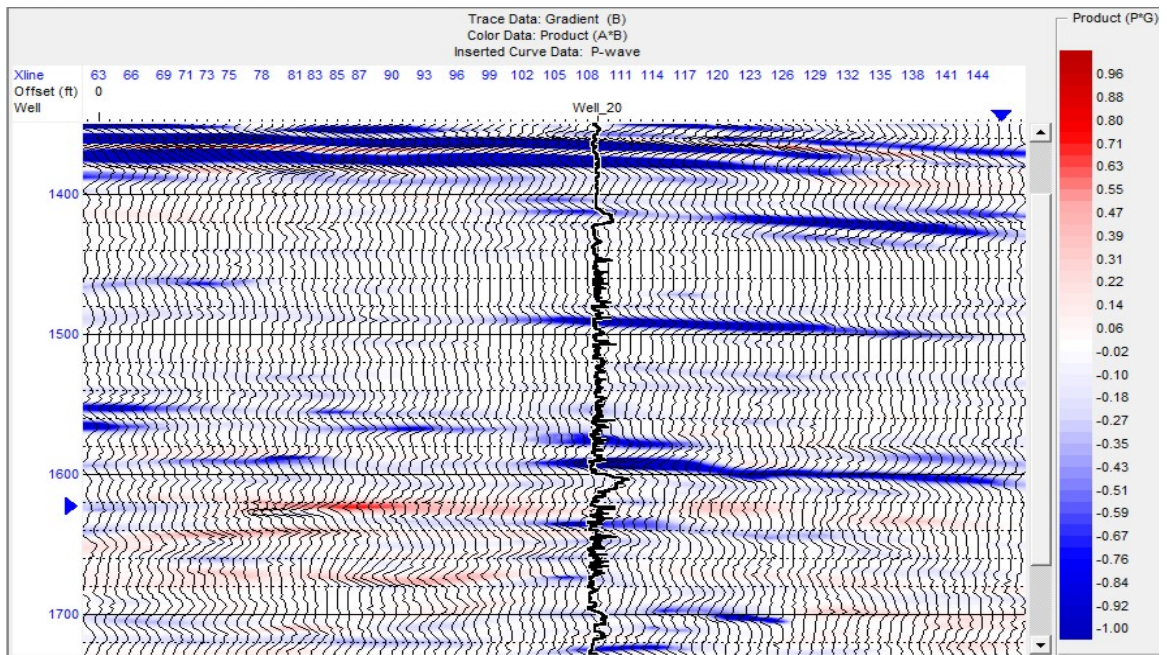


Figure 4-7: Gradient section generated from the AVO volume.

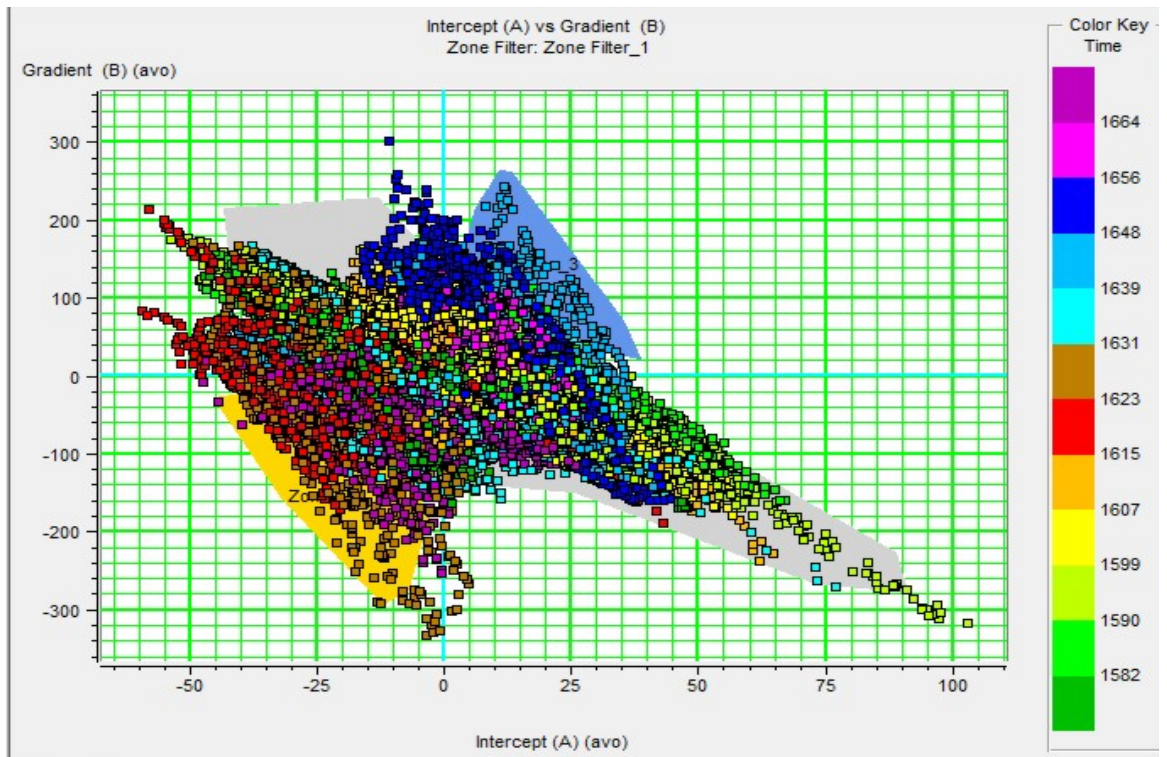


Figure 4-8: Crossplot intercept vs. gradient.

4.2.2 Post-stack Seismic Inversion:

After finishing the AVO analysis, we moved forward to the inversion process to enhance the vertical resolution in the CDP stack section we have.

We decided to perform a model-based inversion to obtain an acoustic impedance model of the reservoir zone. We used the Hampson-Russell STRATA module for this purpose. We loaded the CDP stacked version we created during the processing step. We used the well logs database, where we have all the necessary logs needed to create an impedance volume.

The model-based inversion is based creating an initial model and use multiple iterations to enhance this model and get the least errors possible.

We followed the following steps to perform the inversion process on STRATA:

1. Create an acoustic impedance initial model using the available logs.
2. Use the inversion error analysis tool in the STRATA module to reduce the QC the model.
3. Perform post-stack inversion to receive the final acoustic impedance model of the reservoir zone.

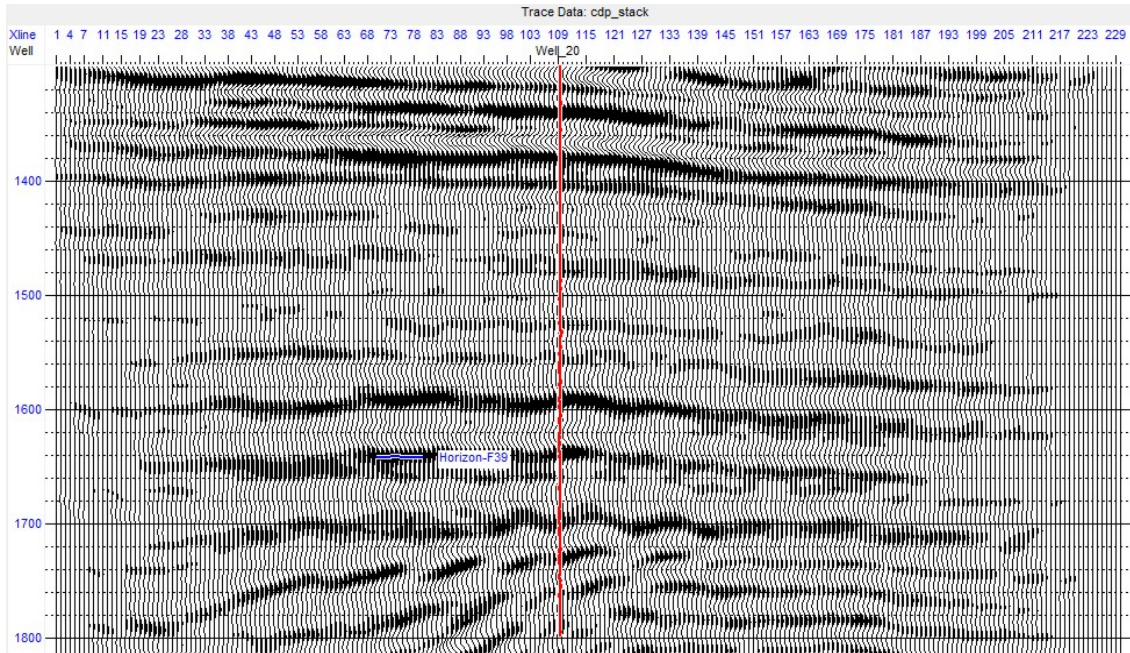


Figure 4-9: CDP-stacked section, input to the inversion process.

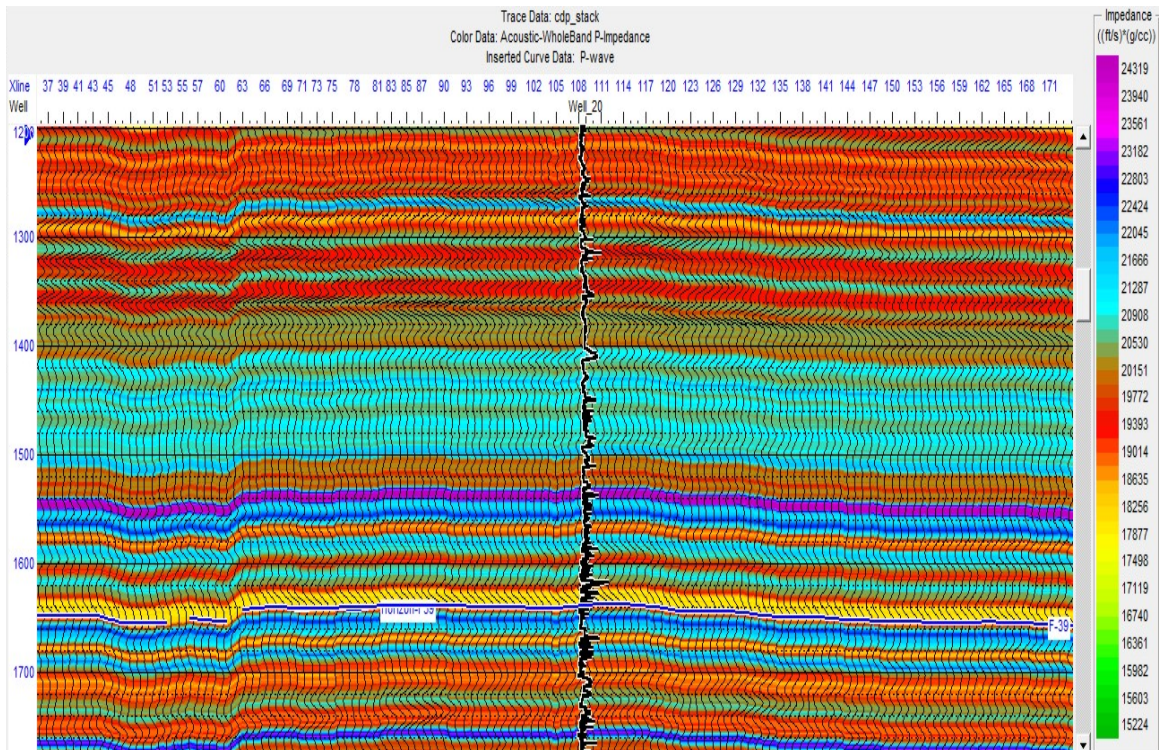


Figure 4-10: Post-stack initial inversion model.

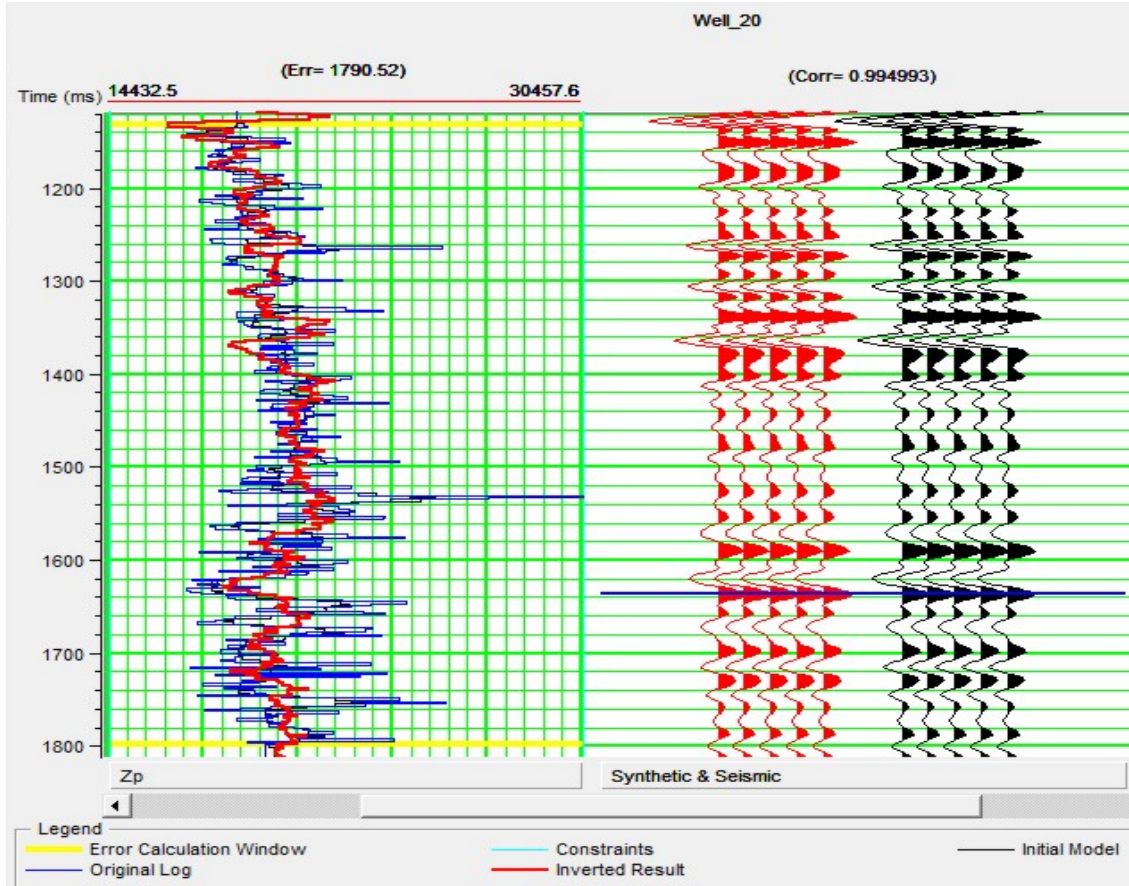


Figure 4-11: Inversion error analysis. Correlation between initial model and final model is 0.99.

We followed these steps and created an acoustic impedance model. On this model it was easier to see the anomalies and to interpret the section using the impedance volume. But the results were not very satisfying. So, we decided to move forward with the pre-stack inversion and creating an elastic impedance model and LMR attributes.

4.2.3 Pre-stack Seismic Inversion:

We decided to move forward to the Pre-stack inversion to get better results of the inversion. Pre-stack inversion is known to be a long process that consumes a lot of computing power and processing time. So we had to cut the data to fit about the reservoir zone only to reduce the processing time.

We followed the same steps for the post-stack seismic inversion; only in the pre-stack inversion the V_s (S-wave velocity) is needed. We used the Castagna's mudrock line equation to create this log. The output of this process can produce: acoustic wave impedance volume, S-wave impedance volume, P-wave velocity volume, S-wave velocity volume, density volume, and a (V_p/V_s) volume. The results showed anomalies at the reservoir zone, but could not help to reveal the rest of the reservoirs above the zone of interest.

Traditional AVO and petrophysical analysis hunts for anomalous variations in P-wave and S-wave velocities, to indicate primarily changes in pore fluid and lithology. The emphasis of using seismic wave velocities and densities arise from the Knott-Zoeppritz equations for continuity of displacement and stress across an interface. But, looking at the wave equation we cannot find velocities in it. More we find is the ratio of the density to the plane wave modulus. ($M = \lambda + 2\mu$).

As a result, one might think of converting the velocity measurements into Lamé parameters. This method offers an improved identification of reservoir zones through the enhanced sensitivity to pore fluids from pure compressibility, as well as lithologic

variations represented by fundamental changes in rigidity, incompressibility, and density parameters as opposed to mixed parameters of seismic velocities.

We went ahead and performed the LMR conversion attribute, but the results did not follow the geologic settings of the area. As a result, we did not try to perform it any further in the rest of the project.

Chapter 5: Frequency Dependent Amplitude and Velocity Analysis

5.1 Theory of Frequency Dependence:

Frequency dependence has been observed for a long time by Geophysicists while working with seismic sections. Geophysicists have noticed low frequency seismic anomalies under the reservoir zones (Castagna et al., 2003; Goloshubin et al., 2006).

Recent rock physics models and field data studies (Han and Batzle, 2002; Goloshubin et al., 2006) suggest a frequency dependence on seismic attribute analysis such as AVO. The main point is using the frequency dependent attributes not only as a DHI (Direct Hydrocarbon Indicators), but also more as a tool for the estimation of hydrocarbon saturation.

There are many factors that might cause frequency dependence such as; scattering, velocity dispersion, reservoir thickness, anisotropy of P-waves and S-waves, and the formation density as a function of location $[x,y,z]$. Most papers have agreed on three main reasons: scale effect, scattering, and intrinsic attenuation.

The physical properties of a medium depend on the scale we use for our investigation. If we change the scale of investigation, we change the intrinsic properties of the reservoir.

Frequency dependent AVO analysis has been discussed and utilized in different papers. Mainly there are three classes for a frequency dependent AVO anomaly; low

frequency dim-out, phase reversal, and low frequency bright spot (Ren et al., 2009; Liu et al., 2011).

In most of the papers we encountered, the main reason for frequency dependence was either: attenuation or pore fluid saturation. In this project we were trying to investigate the frequency dependence in our dataset and try to understand it.

5.2 Upscaling and Filtering:

5.2.1 Upscaling:

In order to start investigating the frequency dependent analysis, we need to look at tools that we can use to filter the frequencies in the dataset. There are different tools that could be applied to the seismic data, from using simple band-pass filters to using spectral decomposition with its different algorithms and techniques. For the log data, we needed to perform upscaling on the logs to transfer them from the high frequencies to lower frequencies that can match the filtered seismic sections.

For the well log preparation, we investigated different methods for upscaling. Upscaling means the prediction of the elastic wave velocities at lower frequencies using velocities at higher frequencies. When using elastic waves to study rocks, we need to give a specific consideration to the scale we perform our investigation upon. When we need to perform our investigation on a smaller scale, we need to use higher frequency, as frequency is inversely proportional to the wavelength.

At the moment, there are 3 main ways to perform upscaling; simple averaging, Backus averaging, and pair correlation function (PCF). (Tiwary, et al., 2009).

Simple averaging is a calculation of average values of elastic moduli and density of the layers within a given window.

The Backus method assumes a thin-layered medium, the exact solution to the effective stiffness tensor can be found. The Backus method also assumes the medium within the given window is layered.

PCF method makes it possible to calculate a frequency dependent stiffness tensor via the PCFs found for the heterogeneous medium and dynamic Green's tensor constructed for a respective medium having average properties (Tiwary, et al., 2009).

The difference among these methods is related to the physical background. The Backus and PCF methods have an underlying physical model, yet Backus succeeds to model the frequency dependence due to the scale effect.

It is difficult to decide which method would give better results for a particular case. Ren et al. (2009) suggest that a comparison should be done between the experimental results and field results to determine which methods would give better results once used. We decided to use the Backus method in this project since it accounts for the scale effect, and is widely used in the industry.

We started our frequency dependent velocity analysis by working on the well logs to investigate frequency dependence in the dataset. We used the Backus algorithm to smooth the logs and measure different velocities at different frequencies.

We needed to investigate different frequencies. So we used the Backus averaging to reproduce sonic logs at 10Hz, 20Hz, 30Hz, 40Hz, and 50Hz. It is worth mentioning that the lower the frequency, the lower the output velocity is specially at the reservoir zone. We saw the lowest velocity at the 10Hz and 20Hz, while almost the same velocity for 40Hz and 50Hz.

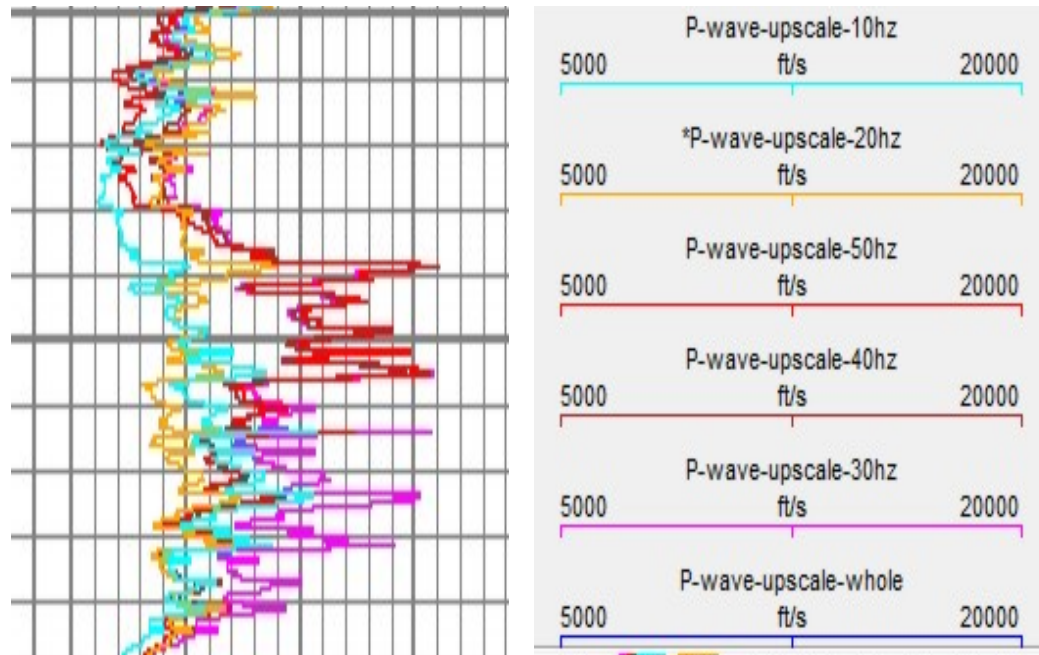


Figure 5-1: On the right, upscaling performed using Backus method. Low frequencies have lower velocities at the reservoir zone. To the right, a diagram with the colors of different logs represented on the left.

5.2.2 Data Filtering:

To start the amplitude analysis, the dataset had to be modified to match the requirements of the processing techniques. We used the same filtered chunks we created during our velocity analysis for our amplitude analysis.

Each filtered chunk was then correlated to its matching sonic log that was created using the Backus averaging method. Wavelets were extracted from each chunk, where each wavelet has 200ms wavelength and extracted from 1300-1800ms. The extracted wavelets had a Ricker-wavelet shape, with zero phase and 2 side lobes.

Center Frequency	Low-cut	High-Cut	Bandwidth
10	0-8	12-20	20
20	0-16	24-40	40
30	0-24	36-60	60
40	0-32	48-80	80
50	0-40	60-100	100

Table 5-1: Filtering parameters for every center frequency.

Reflectivity series was then calculated and correlated to the filtered seismic sections, individually. Each frequency-filtered chunk had a higher correlation coefficient between the logs and the seismic than the original correlation coefficient generated between the logs and the unfiltered seismic section.

5.3 Frequency Dependent AVO Analysis

After we prepared our dataset for a frequency dependent AVO analysis, we were ready to perform the analysis. We would like to mention that the exactly same steps were repeated for every filtered chunk.

We loaded the filtered CDP gathers into the Hampson-Russell AVO module, we then started our analysis by AVO modeling using a single well, where we used well 20 for the modeling.

After the wavelet extraction, and the seismic-log correlation, we picked the horizon of interest at the top of the reservoir zone (1642ms). We then viewed a pick analysis to see how the amplitude changes along the horizon.

We used the correlated sonic log to create an angle gather, where the maximum angle at the zone of interest was 33° . We created these angle gathers to be used for the pre-stack seismic inversion later on.

For every filtered chunk, we created an AVO volume to be processed to produce the intercept and gradient sections for every chunk. The output gradient and intercept sections were then cross-plotted to identify the type of AVO anomaly we are investigating. We used the exact same zones that were created for the unfiltered seismic section to ensure a fair comparison. We had class III AVO anomalies. These bright spots were then mapped on the seismic section using the crossplots on the CDP-stacked sections. We noticed that different frequencies give different results, most probably due to scale effect and resolution.

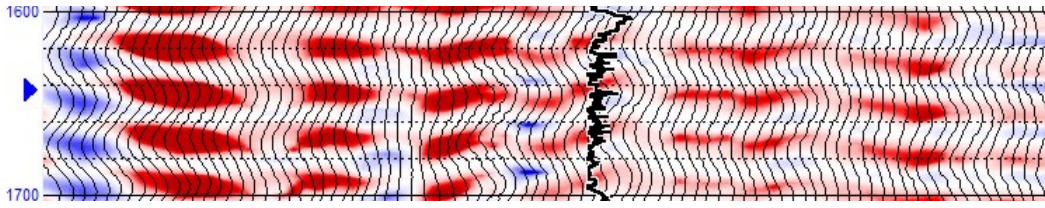


Figure 5-2: Intercept section for the 20Hz-filtered section.

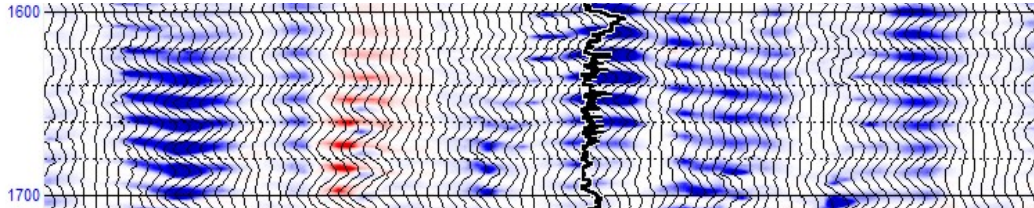


Figure 5-3: Intercept section for the 40Hz-filtered section.

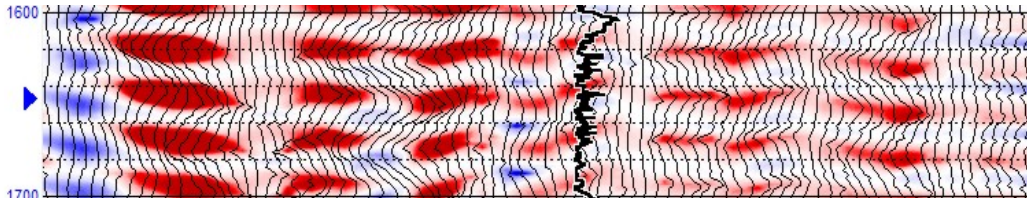


Figure 5-4: Gradient section for the 20Hz-filtered section.

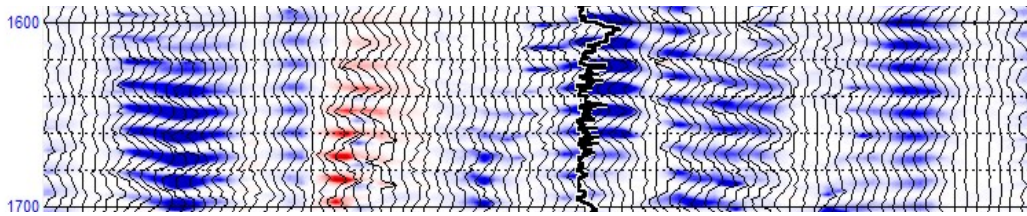


Figure 5-5: Gradient section for the 40Hz-filtered section.

5.4 Frequency Dependent Pre-stack Inversion

Inversion as stated earlier is the process of creating a model of the subsurface using surface measurements. Inversion eases the process of interpretation and structural mapping by creating impedance models that respond better to the reservoir zones. Inversion is also an integration process, which enhances the SNR (Signal to Noise Ratio) and gets rid of the effect of lobes of the seismic wavelet.

Since inversion enhances the vertical resolution, we needed to take a look at the pre-stack inversion results of the filtered data chunks to see which frequency maps the reservoir better. Another advantage for the use of the pre-stack inversion is: it helps the seismic interpreter by producing: acoustic wave impedance volume, shear wave impedance volume, density volume, and angle gather synthetics. By comparing these volumes side-by-side, a seismic interpreter can easily identify the reservoir zone and map the anomalies.

We used the Hampson-Russell STRATA module to perform the pre-stack inversion process. Instead of using the filtered CDP gathers, we used the corresponding angle gathers for every filtered section. We then proceed to a model-based inversion technique.

We use the available log data to create an initial model for the inversion process. This initial model is iteratively corrected and enhanced to reduce error and noise.

After creating the initial model, we start to perform the error analysis and correcting the regression coefficients to ensure the lowest possible error. Then a

percentage of the error is displayed. If the error percentage is minimal we choose to perform the inversion process. If the error is too large, one might decide to correct the model and the regression coefficients to decrease the error. During our analysis, the error did not go past 10%, which gave us satisfying results.

To decrease the processing time, we only performed the inversion process on the 1300-1800ms chunk, from inline 74-76 while including all the crosslines. This was done since we were only modeling well 20 that falls into inline 75 and crossline 109. The main aim behind cutting down the data was to reduce the processing time, as we were going to perform the pre-stack inversion 5 times for 5 different sections.



Figure 5-6: Pre-stack inversion model, 10Hz.

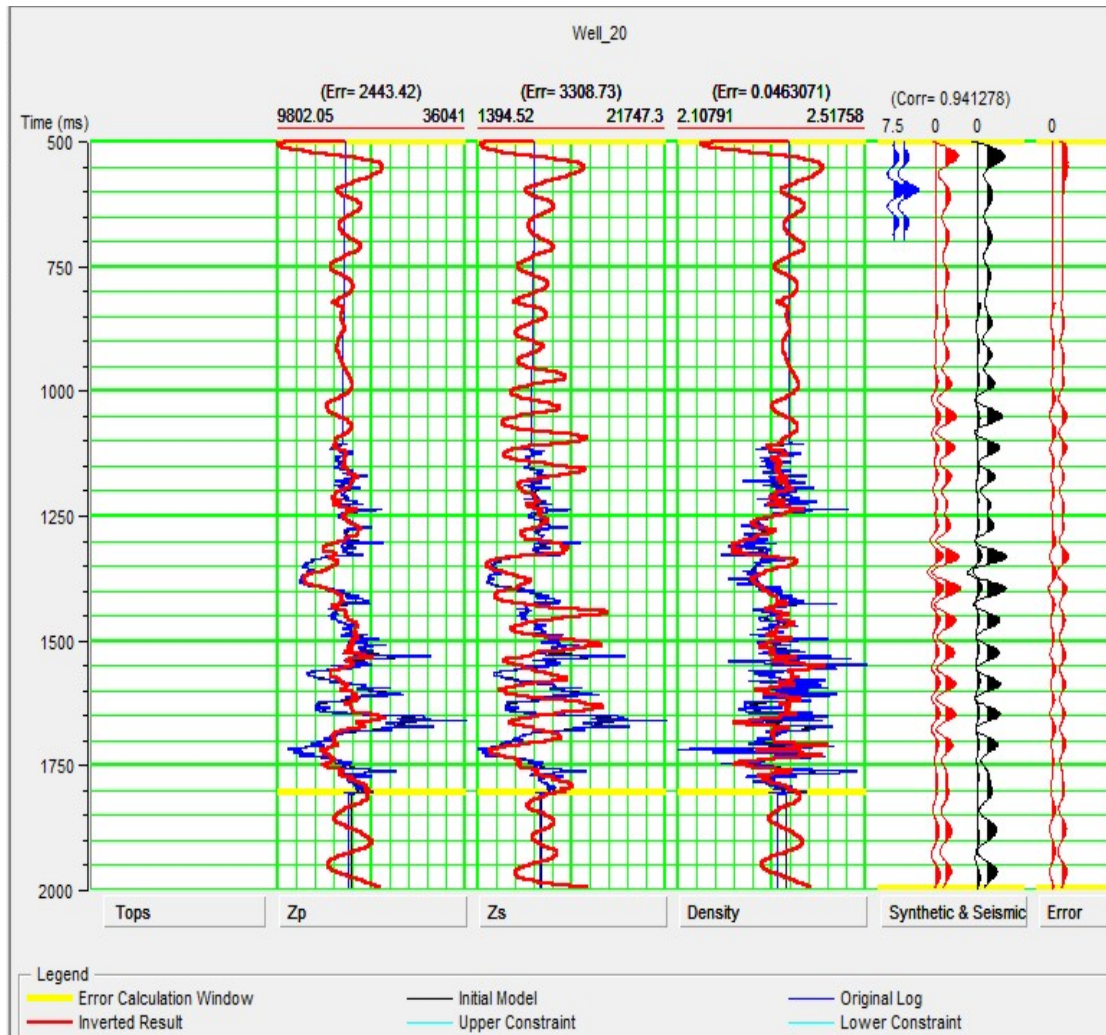


Figure 5-7: Pre-stack inversion error analysis. Correlation coefficient between initial and final model is 0.94.

The outputs of the inversion results were: volumes of acoustic wave impedance, shear wave impedance, density, and angle gather synthetics for every filtered chunk. These volumes helped us to interpret the reservoir zone and judge which frequency could map the reservoir better.

Chapter 6: Results

In this chapter we discuss the results we obtained from the different stages of our investigation. We compare the different results of the different analyses and discuss these results.

We will display and discuss the results of the following analyses: frequency dependent amplitude analysis, frequency dependent velocity analysis, and frequency dependent inversion results.

6.1 Frequency Dependent Amplitude Analysis:

We performed our amplitude analysis on the unfiltered dataset, and the filtered versions with different center frequencies (10Hz, 20Hz, 30Hz, 40Hz, and 50Hz).

The CDP gathers and angle gathers ensure that the filters applied are working properly. The wavelets extracted from the filtered seismic sections show a band wide enough to have a wavelet with minimum side lobes.

The AVO results from the unfiltered section, 20Hz-filtered section, and 40Hz-filtered section are compared. We used the same zones for the crossplots of the intercept and gradient of each corresponding AVO volume.

We found out that although the unfiltered section did not map the reservoir at 1642ms, it showed the reservoirs above and below. The 20Hz section successfully mapped the reservoir zone at 1642ms and also showed the reservoirs above and below. The 40Hz section failed to show the reservoir similar to the unfiltered section. It did show the reservoir above, but failed to show the one below.

As a result, we think that the low frequencies map the reservoir better. And to increase the vertical resolution, we will display the results of the inversion process. But first, we need to take a look on the velocity analysis.

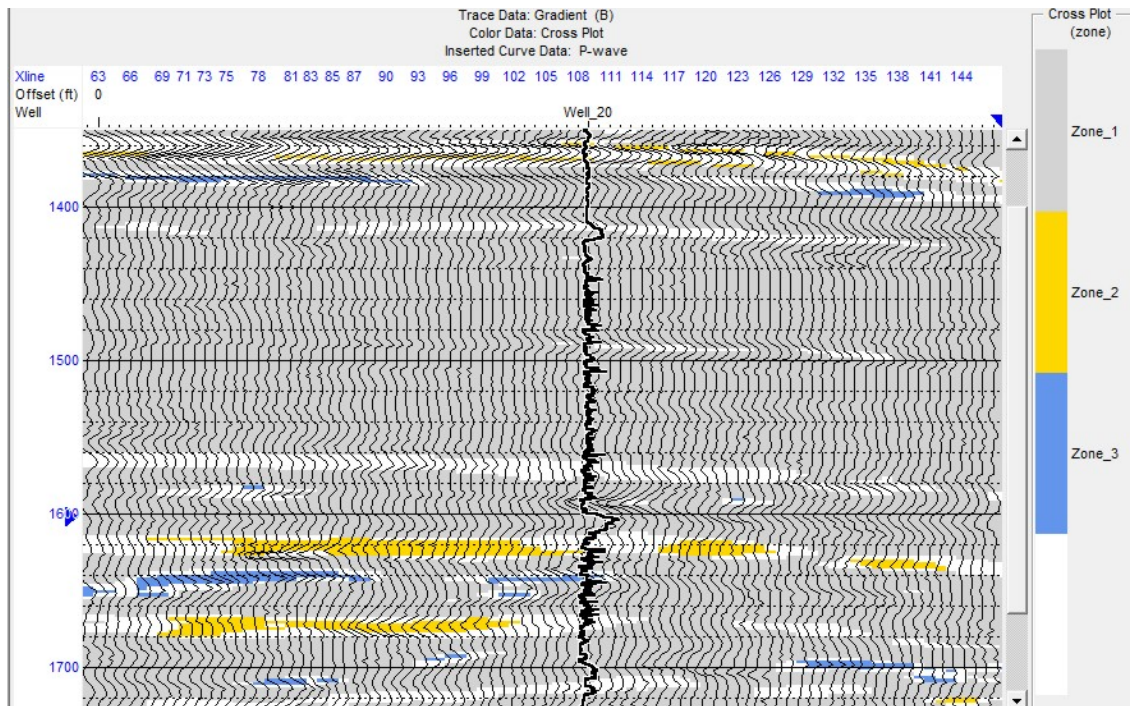


Figure 6-1: Intercept and gradient crossplot for the unfiltered section (whole frequency band). No amplitude anomalies noticed at the reservoir zone.

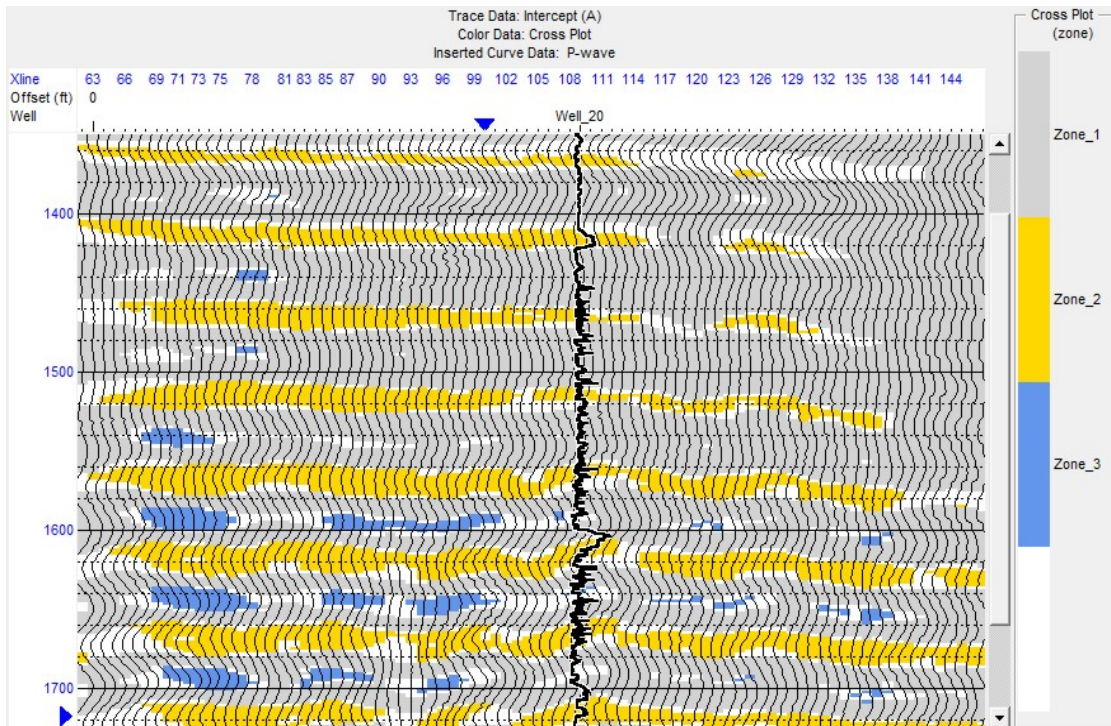


Figure 6-2: Intercept and gradient crossplot for the 20Hz-filtered section. Amplitude anomalies noticed at the reservoir zone.

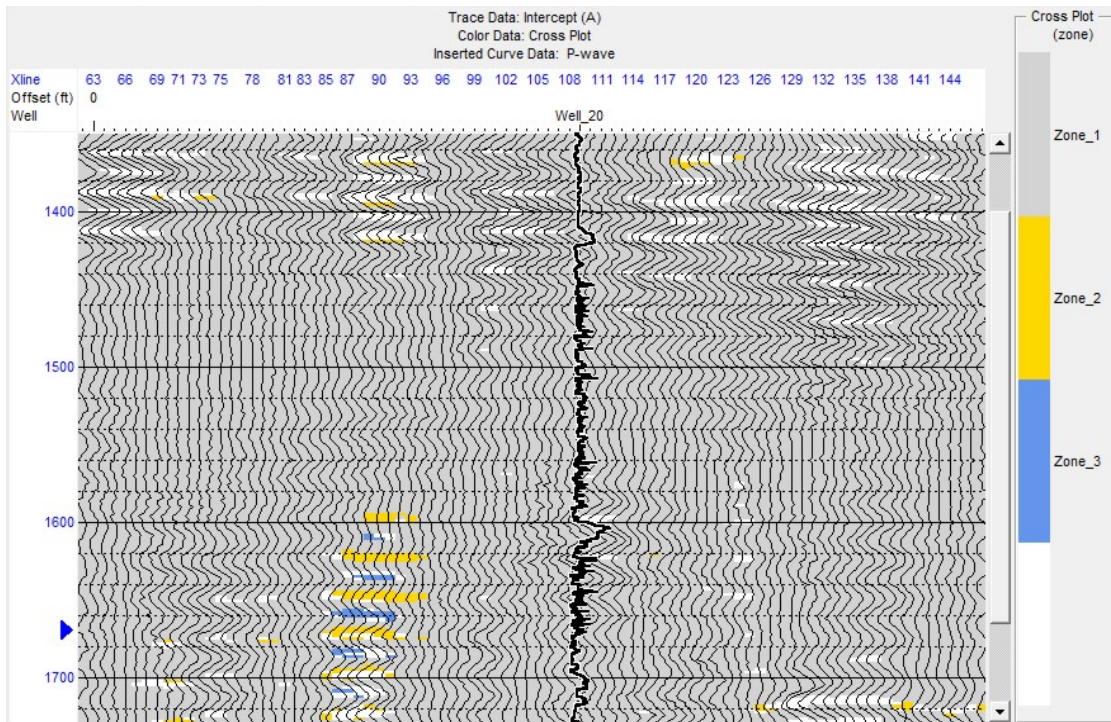


Figure 6-3: Intercept and gradient crossplot for the 40Hz-filtered section. Amplitude anomalies are noticed further to the left of the drilling location.

6.2 Frequency Dependent Inversion Results:

The main aim behind performing the inversion process is to enhance the vertical resolution, and produce impedance models that can help us identify and map the reservoir zone in a better way.

The post-stack inversion produced an acoustic impedance model that showed anomalous behavior at the reservoir zone. The error analysis performed before the inversion produced a 0.99 between the initial model and the inverted model. Yet again, the acoustic model showed the anomalous behavior above the reservoir zone, not at the exact location. The 40Hz model showed the anomalous behavior at the exact location of the reservoir as well as the 20Hz model. Yet, the 20Hz model showed a better anomaly at the reservoir location. These initial results showed that the 20Hz model (the lower frequencies) could map this reservoir in a better way.

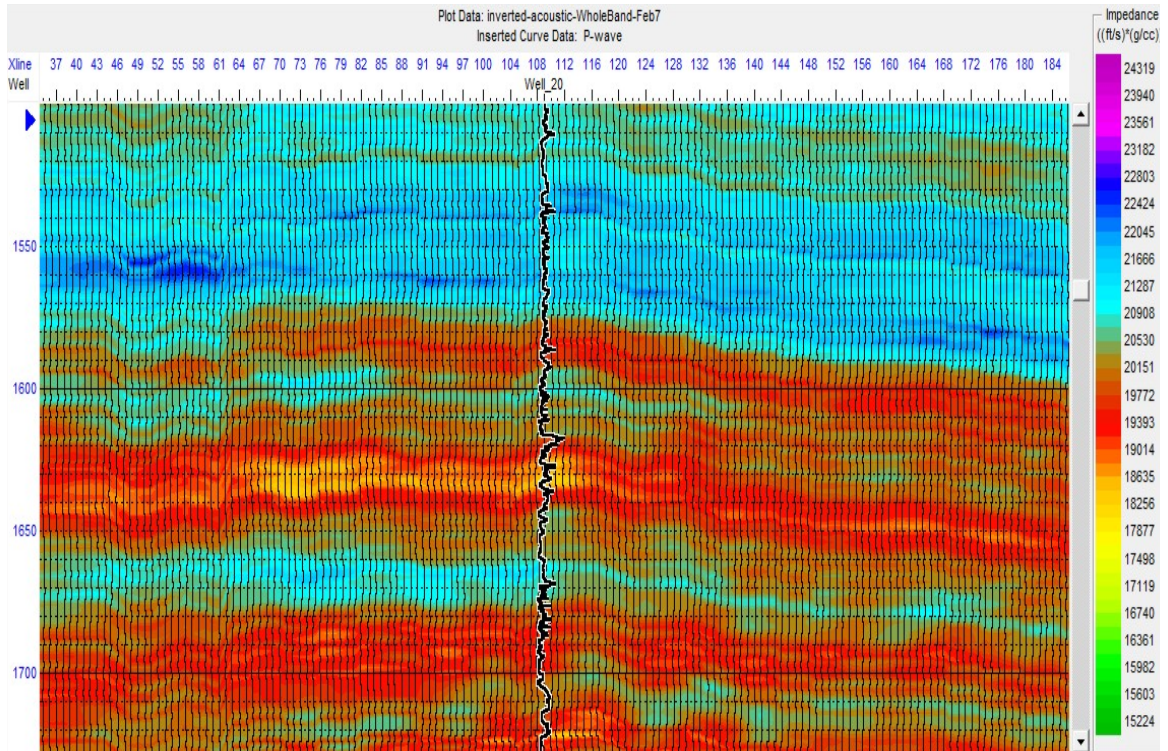


Figure 6-4: Post-Stack seismic inversion for the unfiltered section (whole frequency band). An anomaly is revealed at the reservoir location that was not revealed during the AVO analysis.

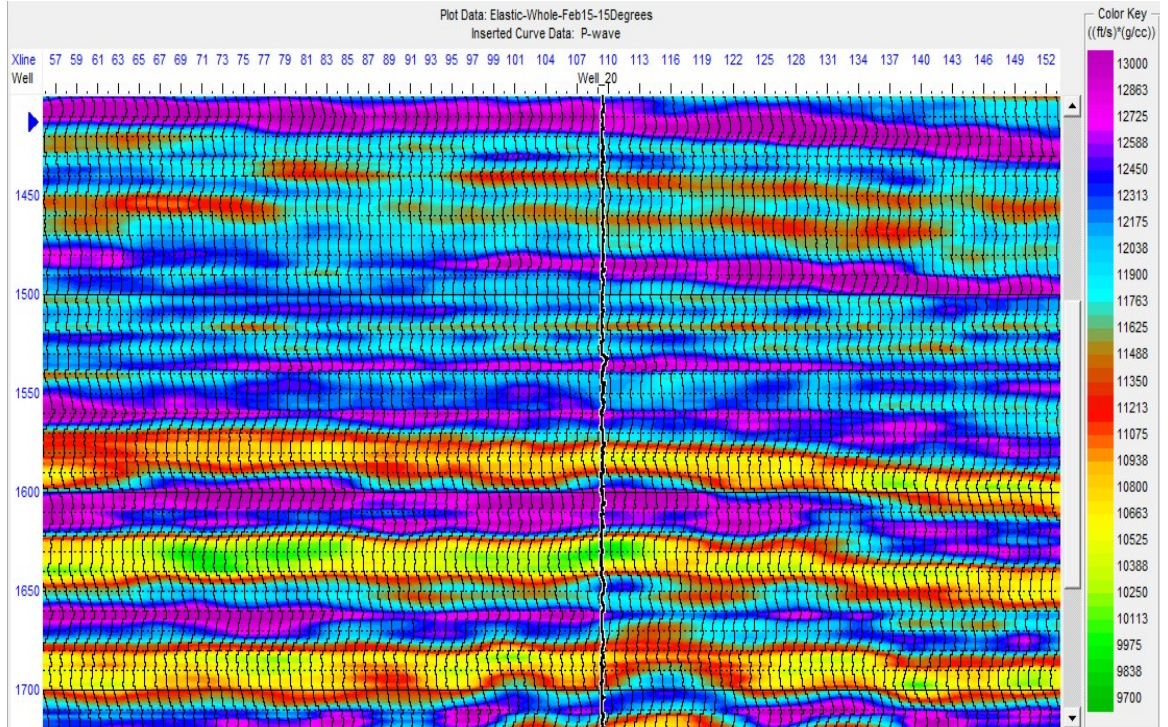


Figure 6-5: Elastic impedance inversion for the unfiltered section (whole frequency band). Same anomaly is revealed as on the acoustic impedance volume.

The pre-stack inversion was then deployed for better results, where we can have an acoustic impedance model, a shear wave impedance model, and a density model, and we can view the angle gathers synthetics at the reservoir zone. This process was repeated for all the frequencies (10, 20, 30, 40, and 50Hz).

The 10Hz model gave a correlation coefficient of 0.94 between the initial model and the inverted model. As for the post-stack inversion, it gave an anomalous behavior at the reservoir zone. This anomaly was well displayed on the shear wave impedance volume, as well as the density volume.

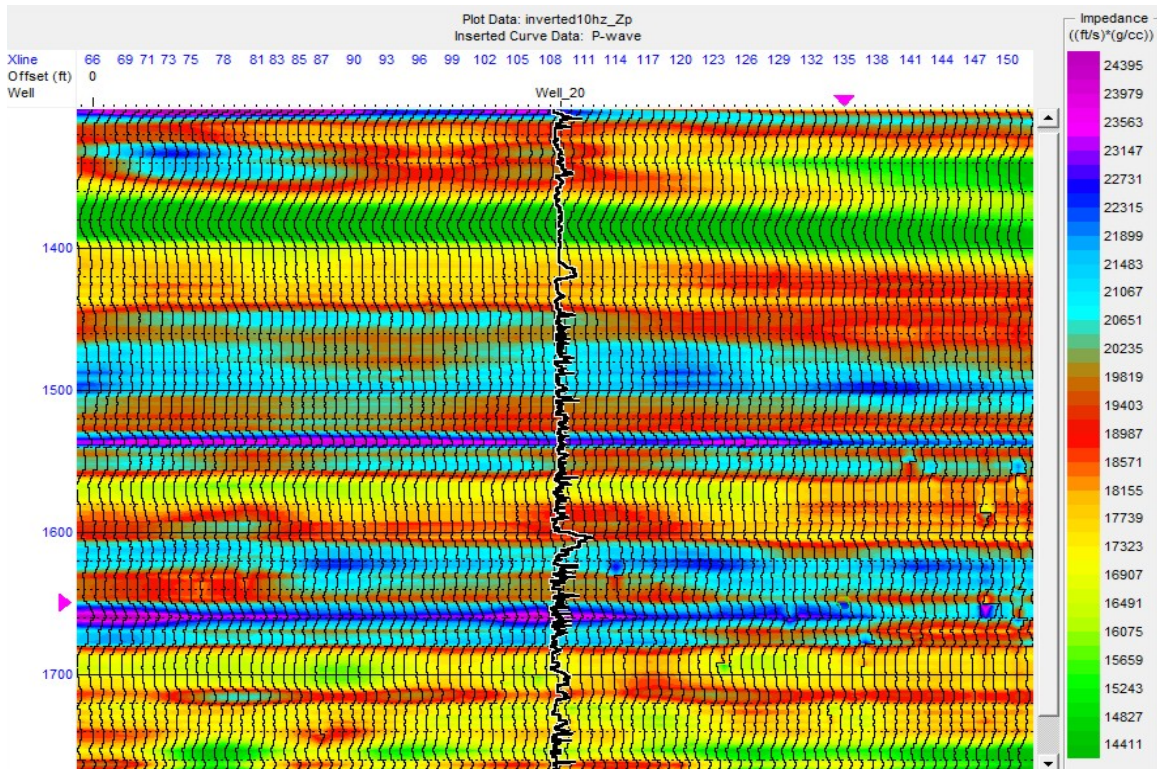


Figure 6-6: Acoustic wave impedance inversion section, 10Hz.

The 20Hz model showed a better correspondence to the acoustic wave impedance, while the shear wave impedance failed to map the reservoir zone. Yet, the density showed an anomaly at the reservoir location.

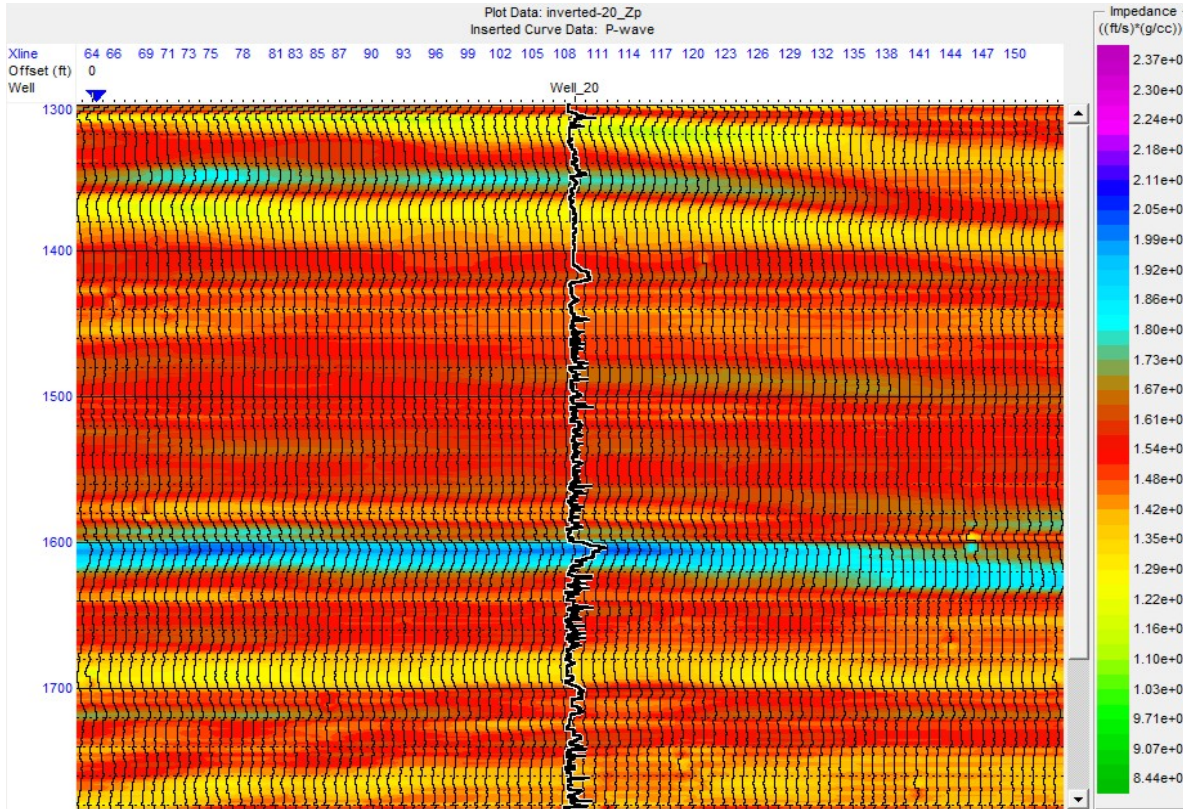


Figure 6-7: Acoustic wave impedance inversion, 20Hz.

The 30Hz model showed anomalous behaviors at the location of the reservoir zone in both models; acoustic wave impedance volume, and shear wave impedance volume. Yet, the anomaly was flat and did not follow the geology of the area revealed in previous 10Hz model. The density volume showed an anomaly that has higher densities than in the 10Hz and 20Hz density volumes.

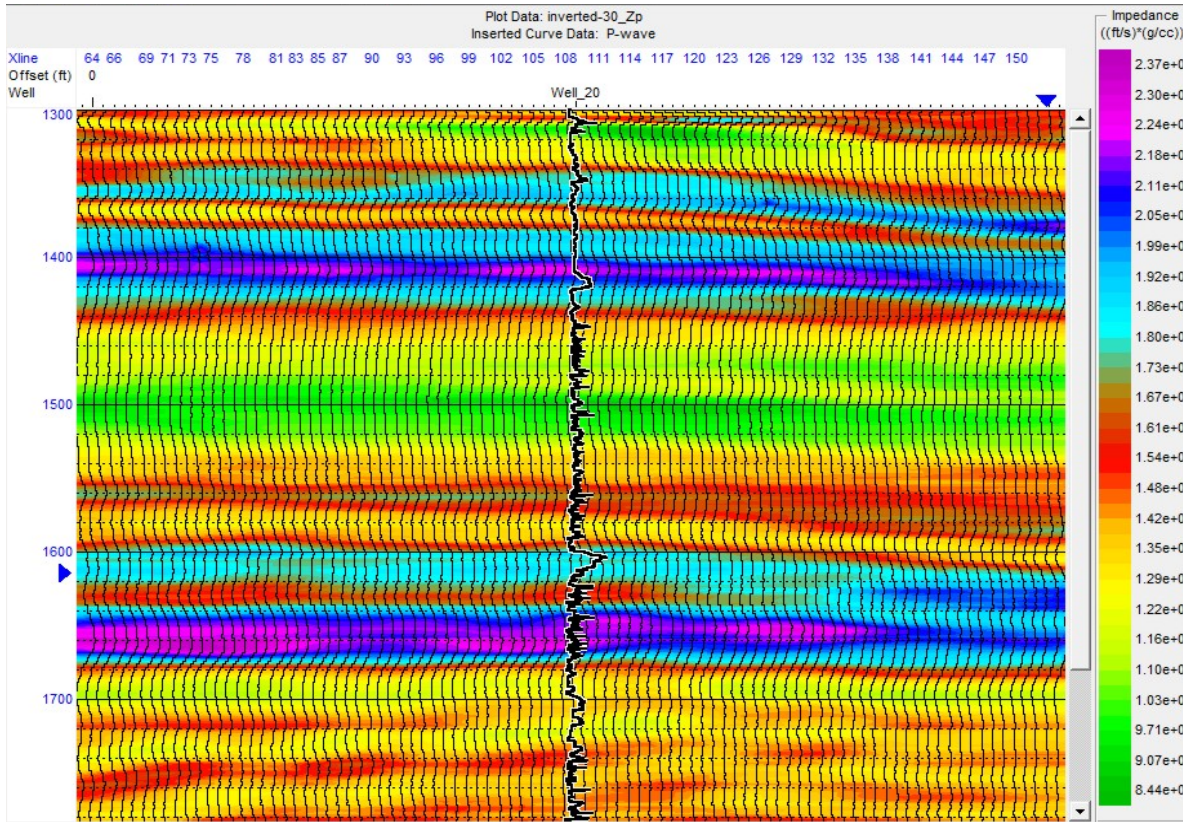


Figure 6-8: Acoustic wave impedance inversion, 30Hz.

The 40Hz model and the 50Hz model showed flat anomalies at the reservoir zone for the acoustic wave impedance model, and the density volume that did not respond to the geology of the area. Yet, it failed to show any anomalous behaviors for the shear wave impedance model at the reservoir zone.

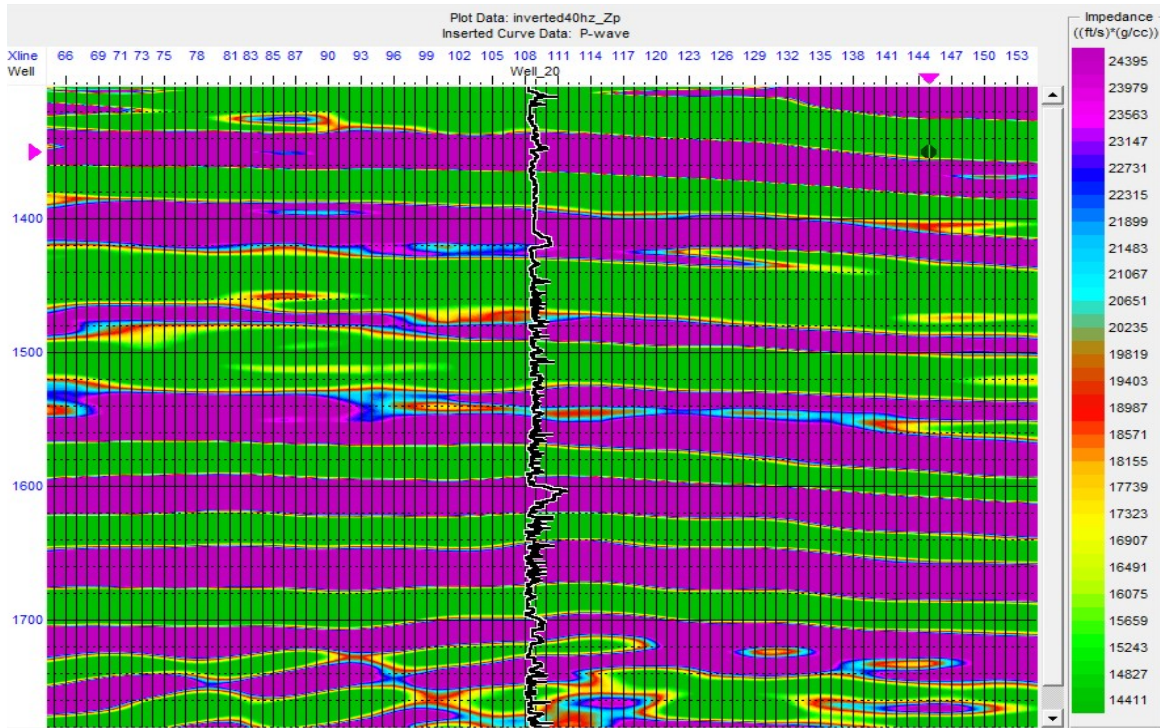


Figure 6-9: Acoustic wave impedance inversion, 40Hz.

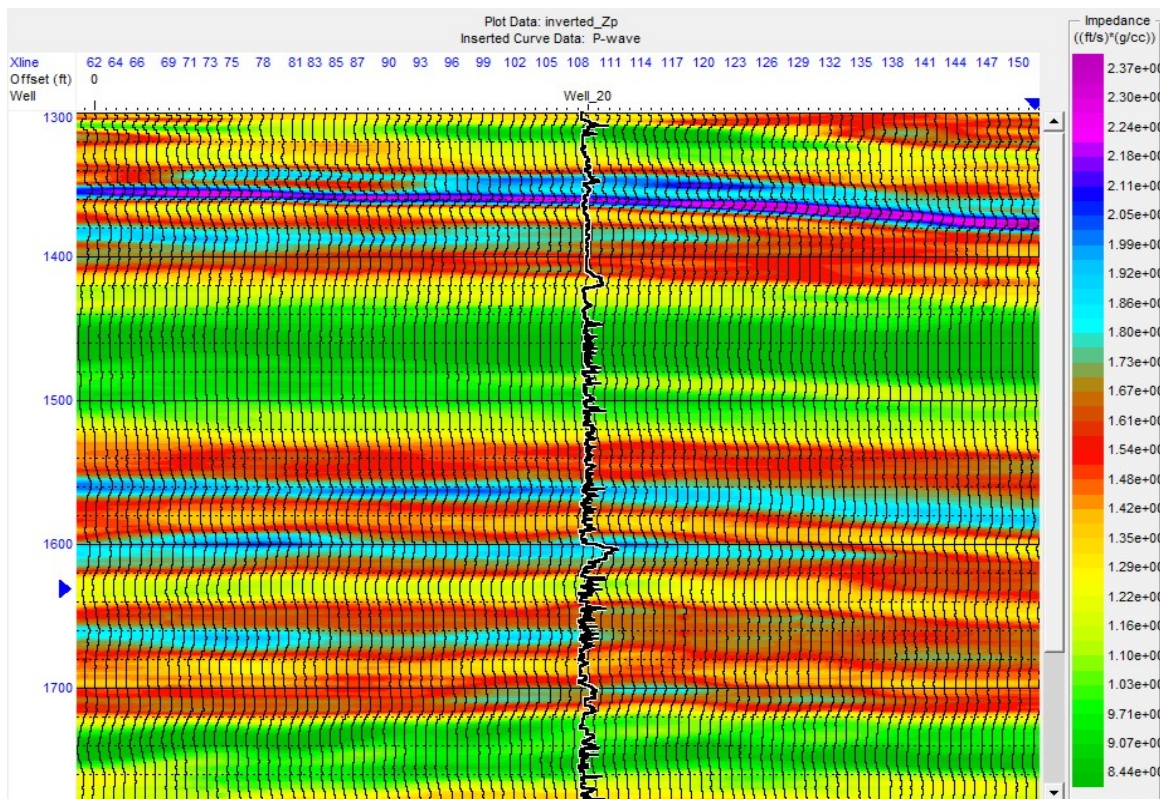


Figure 6-10: Acoustic wave impedance inversion, 50Hz.

The 10Hz model corresponded very well to the reservoir zone in terms of the acoustic wave impedance model, the shear wave impedance model, and the density model.

As we can see from the previous results, the 10Hz model was the most successful model in mapping the reservoir.

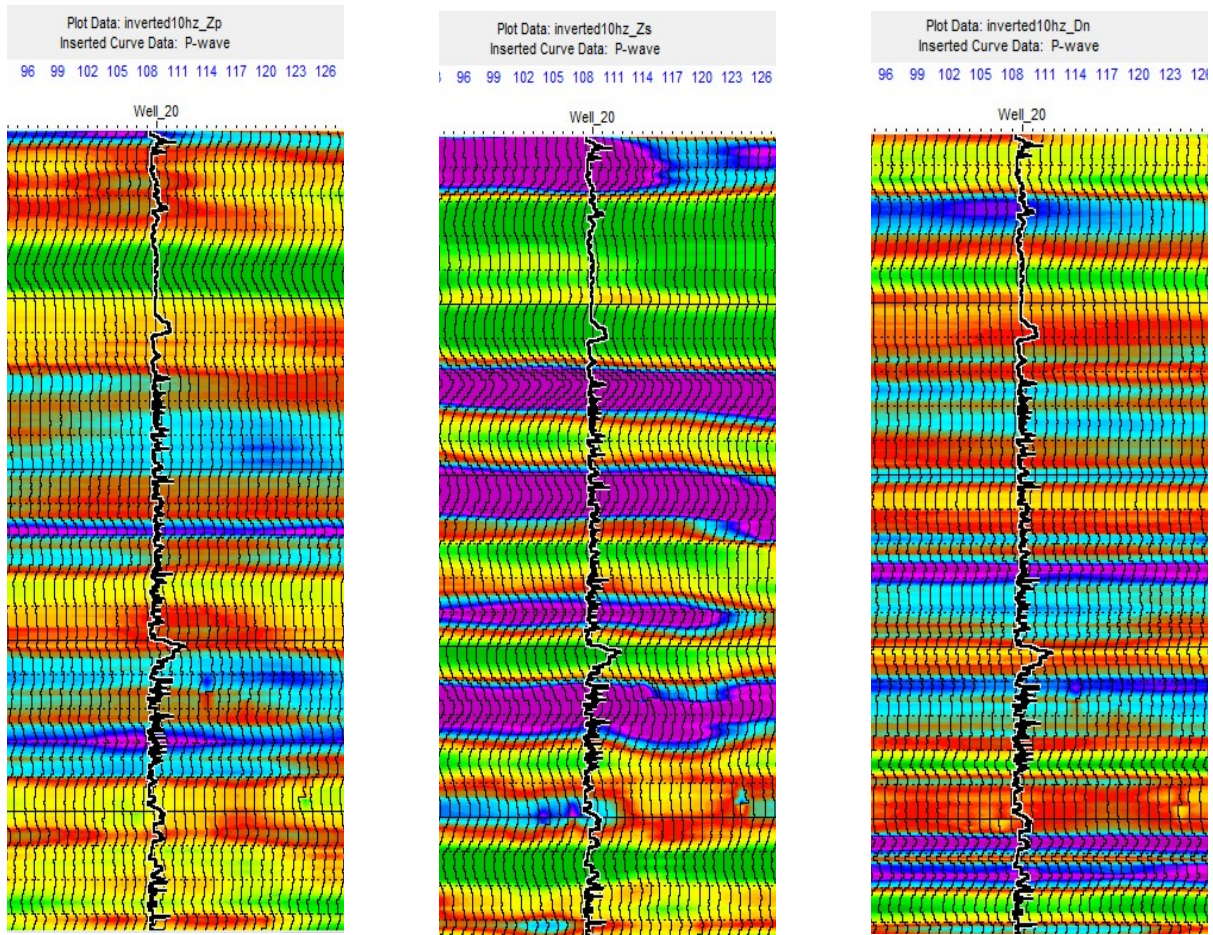


Figure 6-11: 10Hz Pre-stack inversion volumes. On the left, acoustic wave impedance volume. In the middle, shear wave impedance volume. On the right, density volume.

Conclusion:

We followed the conventional analysis methods to investigate the reservoir F-39 at 6800ft subsea. The conventional methods could not reveal the reservoir characteristics, and mapping the reservoir using AVO analysis was not effective. The post-stack inversion enhanced the resolution to some extent, yet it did not reflect the real thickness of the reservoir.

As the utilization of conventional analysis failed to help us identify the reservoir, we decided to perform a frequency dependent analysis.

We filtered the dataset into 5 different center frequencies, and we performed a frequency dependent amplitude analysis, and velocity analysis. We used Backus averaging method to smooth the well logs in order to match them to the filtered seismic data. The upscaling of the well logs revealed a much slower velocity for the low frequencies at the reservoir zone.

The AVO analysis, in particular the cross plot technique, showed better results for lower frequencies. Then we decided to perform a pre-stack inversion process so we can have impedance and density volumes that can help us identify and map the reservoir zone in a better way.

The pre-stack inversion showed significant results at the low frequencies, while the high frequencies failed to map the reservoir. The acoustic wave impedance volumes for the higher frequencies failed to map the reservoir, and the shear wave impedance did

not provide any additional details. One might consider the validity of the shear wave impedance volumes since they are built basically from the acoustic impedance volume empirically using the Castagna's mudrock line equation.

The 10Hz model was the most successful in terms of mapping the reservoir zone.

We therefore, relate the low frequency success to map the reservoir to the saturation of hydrocarbons in the reservoir. We think that the hydrocarbons attenuate the higher frequencies much faster than the low frequencies, which first causes velocity dispersion, and high attenuation at higher frequencies. Also switching the center frequency of the dataset by means of filtering will lead to revealing of different structural features and different resolution. The higher frequencies provided higher resolution, but the lower frequency showed the reservoir zone in a better way.

We conclude at the end of our project that frequency dependent analysis can help the seismic interpreter to better understand the structural features of the area, and can help to map the reservoir zone in a better way. We also recommend a processing technique that is both amplitude and frequency preserving. Seismic processors tend to neglect the low frequencies as they are very much contaminated with different types of noise, but as we see in this project, the 10Hz model was more successful than the higher frequencies in identifying and mapping the reservoir.

References:

- B. A. Hardage, R. A. Levey, V. Pendleton, J. Simmons, and R. Edsen, A 3-D seismic case history evaluating fluviially deposited thin-bed reservoirs in a gasproducing property. *Geophysics*, 59, p. 1650-1665.
- H. El-Mowafy, K. J. Marfurt, Structural interpretation of the middle Frio Formation using 3D seismic and well logs: An example from the Texas Gulf Coast of the United States. *The Leading Edge*, July 2008.
- H. El-Mowafy, and K. Marfurt, Integration of 3-D seismic attributes and sequence stratigraphy in interpreting the middle frio formation fluvial architecture. case history: Stratton and Agua Dulce Fields, South Texas, USA. SEG/New Orleans 2006 Annual Meeting.
- W. J. Ostrander, 1984, Plane-wave reflection coefficients for gas sands at non-normal angles of incidence: *Geophysics*, 49, p. 1637-1648.
- C. P. Ross, 2000, Effective AVO crossplot modeling: A tutorial, *Geophysics*, 65, p. 700-711.
- C. P. Ross, and D. L. Kinman, 1995, Non-bright-spot AVO: Two examples, *Geophysics*, 60, p. 1398-1408.
- P. N. Mahob, and J. P. Castagna, 2003, AVO polarization and hodograms: AVO strength and polarization product, *Geophysics*, 68, p. 849-862.
- S. R. Rutherford, R. H. Williams, Amplitude-versus-offset variations in gas sands, *Geophysics*, 54, p. 680-688.

- J. P. Castagna, H. W. Swan, and D. J. Foster, Framework for AVO gradient and intercept interpretation. *Geophysics*, 63, p. 948–956.
- P. Connolly, BP, Elastic impedance. *The Leading Edge*, April 1999.
- R. D. Martinez, Wave propagation effects on amplitude variation with offset measurements: A modeling study. *Geophysics*, 66, p. 1284–1293.
- G. Goloshubin, and D. Silin, Frequency-dependent seismic reflection from a permeable boundary in a fractured reservoir. *SEG/New Orleans 2006 Annual Meeting*.
- J. P. Castagna, ARCO Oil and Gas Company, Petrophysical imaging using AVO. *The Leading Edge*, March 1993.
- D. Sarkar, J. P. Castagna, and W. J. Lamb, AVO and velocity analysis. *Geophysics*, 58, p. 534-543.
- B. H. Russell, “Introduction to seismic inversion methods”, *SEG continuing Education Short Course*, 1991.
- O. A. Cooke, and W. A. Schneider, Generalized linear inversion of reflection seismic data, *Geophysics*, 48, p. 665-676.
- H. Ren, G. Goloshubin, and F. J. Hilterman, Poroelastic analysis of amplitude-versus-frequency variations. *Geophysics*, Vol. 74, No 6, p. 41-48.
- D. K. Tiwary, I. O. Bayuk, A. A. Vikhorev, and E. M. Chesnokov. Comparison of seismic upscaling methods: From sonic to seismic. *Geophysics*, 74, p. 3-14.
- S. Yoo, and R. L. Gibson Jr., Frequency Dependent AVO analysis after target oriented stretch correction. *SEG/Houston 2005 Annual Meeting*.

- J. P. Castagna, H. W. Swan, Principles of AVO crossplotting. The Leading Edge, April 1997.
- L. Liu, S. Cao, and L. wang, Poroelastic analysis of frequency-dependent amplitude-versus-offset variations. Geophysics, 76, p. 31-40.